ELSEVIER

Journal of Chromatography A, 795 (1998) 133–184

JOURNAL OF CHROMATOGRAPHY A

Review

Diffusion, adsorption and catalytic studies by gas chromatography

Nicholas A. Katsanos[a,*], Richard Thede[b], Fani Roubani-Kalantzopoulou[c]

[a]*Physical Chemistry Laboratory, University of Patras, 26500 Patras, Greece*
[b]*Department of Chemistry, University of Greifswald, Soldmannstr. 23, D-17489 Greifswald, Germany*
[c]*Department of Chemical Engineering, National Technical University of Athens, 15780 Zografou, Greece*

Received 12 June 1997; received in revised form 9 September 1997; accepted 11 September 1997

Abstract

Three topics important in many areas of physical chemistry, namely measurements of diffusion coefficients, adsorption kinetics and adsorption isotherms, as well as rates and conversions in heterogeneous catalysis, are reviewed from the gas chromatography viewpoint. After a general introduction, various theoretical sections include synopses of important mathematical models and developments, followed by experimental sections describing basic instrumentation and set-ups, and sections exemplifying the main results with brief discussions. The article is concluded with a methodology embracing simultaneous determination of all three properties (diffusion, adsorption and catalytic rates) in a single experiment by GC.
© 1998 Elsevier Science B.V.

Keywords: Reviews; Diffusion coefficients; Adsorption; Catalysis; Adsorption isotherms; Kinetic studies

Contents

*Corresponding author.

0021-9673/98/$19.00 © 1998 Elsevier Science B.V. All rights reserved.
PII S0021-9673(97)00968-0

1. Introduction

At first sight, diffusion, adsorption and catalysis may seem to be three independent physicochemical properties, all separate from gas chromatography which is a well-known separation technique. It is not difficult, however, to show that things are not so. For example, the general quantitative relationships in the catalysis of fluid reactions by porous particles, which is the most common situation in heterogeneous catalysis, can be conveniently derived by considering the following four steps in series: (a) the mass transfer of reactants and products to and from the gross exterior surface of the catalyst particle and the main body of the fluid; (b) the diffusional and flow transfer of reactants and products in and out of the pore structure of the catalytic particle; (c) the activated adsorption of reactants and the activated desorption of products at the catalytic interface; and (d) the surface reaction of adsorbed reactants to form adsorbed products [1]. Steps (a) and (b) depend, among other things, on the diffusional characteristics of the fluid; step (c) is strongly dependent on adsorption–desorption phenomena; and step (d) is

determined by the rate of reaction on the catalytic surface. Thus, diffusion, adsorption and surface reaction are closely interconnected in heterogeneous catalysis studies. Many recent studies on tropospheric chemical reactions in the presence of various heterogeneous sinks fall into the same category. Damage functions for the action of air pollutants on historic buildings and monuments, and on cultural heritage kept inside museums and churches, may be quantitatively studied in terms of the four steps described above for catalytic studies [2,3].

The question naturally arising is how, in the examples of studies given above, does gas chromatography enter into play? The answer to this question is simple, since chromatographic separation is a physicochemical process based on convection, diffusion, adsorption and liquid dissolution, and the technique, used today mainly for chemical analysis purposes, cannot possibly 'forget its parents'. Indeed, analysis by GC suffers from the so-called broadening factors, the most important of which are related to non-fulfilment of the assumptions under which the central chromatographic equation is derived, namely: (1) non-negligible axial diffusion of the solute gas in the chromatographic column; (2) non-linearity of the distribution (e.g. adsorption) isotherm; (3) non-instantaneous equilibration of the solute component between the mobile and the stationary phases.

It is through these broadening factors, embraced by the Van Deemter equation, that gas chromatography offers many possibilities for physicochemical measurements, leading to very precise and accurate results with relatively cheap instrumentation and very simple experimental set-ups. These methods are widely used today, a fact emphasized by the publication of two books [4,5] dealing only with such measurements and based on the traditional techniques of elution development, frontal analysis and displacement development under constant gas flow-rate.

Another approach to extract physicochemical parameters from the elution peaks is based on the analysis of the statistical moments of the peaks [6].

The last category depends on perturbations of the carrier gas flow-rate [7], incorporating two techniques: *the stopped-flow* and *the reversed-flow* perturbation. Instead of basing physicochemical measurements on retention volumes of elution peaks, their broadening and their shape distortion due to the physicochemical processes under study, one can perform such measurements accurately and easily if the chromatographic column, being under steady-state conditions, is perturbed so that it deviates from equilibrium for a short time interval and then is left to return to the original state. This procedure is analogous to relaxation techniques.

Let us examine now the three physicochemical properties, namely, *diffusion*, *adsorption* and *catalysis* studied for various systems and solutes by gas chromatographic techniques. Each property examination will include a synopsis of important mathematical models and other theoretical developments, followed by an experimental section describing basic instrumentation and set-ups, and then a section exemplifying the main results with a brief discussion. This article will be concluded by a methodology embracing the simultaneous determination of all three properties in a single experiment by GC.

2. Diffusion in gases

2.1. The broadening technique

The first gas chromatographic method on diffusion measurements was introduced by Giddings and Seager [8] in 1960 and used by many workers both in its original form, as well as in various modified forms. These methods were based on the broadening of the chromatographic elution peaks and have been described in a thorough review by Maynard and Grushka [9] in 1975.

2.1.1. Mathematical model

The mass balance equation of a solute A in an empty GC tube is

$$\frac{\partial c_g}{\partial t} = -\upsilon \frac{\partial c_g}{\partial x} + D_A \frac{\partial^2 c_g}{\partial x^2} + D_A \left(\frac{\partial^2 c_g}{\partial r^2} + \frac{1}{r} \frac{\partial c_g}{\partial r} \right) \quad (1)$$

where c_g = gaseous concentration of A in the tube; t = time; x = length coordinate along the tube; r = radial coordinate of the tube, i.e. distance from the cylinder axis; υ = axial flow velocity of the carrier

gas given by the laminar flow field as $v = 2\bar{v}(1 - r^2/R^2)$, $\bar{v}$ being the mean axial flow velocity and R the tube radius; D_A = binary diffusion coefficient of A into the carrier gas.

The solution of this differential equation, subject to the proper boundary conditions and under certain simplifying assumptions [9], leads to a skewed Gaussian function, which in the limit of a long column of length l and a small carrier gas velocity ($D_A/\bar{v}\,l \leq 0.01$) becomes a Gaussian with a variance, in length units,

$$\sigma_x^2 = \frac{2D_A l}{\bar{v}} + \frac{R^2 \bar{v}\, l}{24 D_A} \tag{2}$$

It is well known that the apparent plate height $\hat{H}$ in chromatography is defined by $\hat{H} = \sigma_x^2/l$ which, substituted into Eq. (2), yields

$$\hat{H} = \frac{2D_A}{\bar{v}} + \frac{R^2 \bar{v}}{24 D_A} \tag{3}$$

This has the same form as the Van Deemter equation

$$\hat{H} = A + \frac{\bar{B}}{\bar{v}} + C\bar{v} \tag{4}$$

ignoring the term A, accounting for flow-independent contributions to $\hat{H}$.

Eq. (3) can be rearranged to form a quadratic equation in D_A, the solution of which is

$$D_A = \frac{\bar{v}}{4}\left[\hat{H} \pm \left(\hat{H}^2 - \frac{R^2}{3}\right)^{1/2}\right] \tag{5}$$

This gives two values for D_A, only one of which has physical meaning. A typical plot of Van Deemter Eq. (4) given in Fig. 1 shows that at slow carrier gas velocities $\bar{v}$ the second term on the right-hand side of Eq. (3) (corresponding to C of Eq. (4)) is small and D_A is determined from the positive root of Eq. (5). At high velocities, the first term of Eq. (3), corresponding to $\bar{B}/\bar{v}$ of Eq. (4), is small and the negative root of Eq. (5) is used to calculate D_A. The crossover point from one root to the other is at the velocity $\bar{v}_{opt}$ minimizing $\hat{H}$. This can be found by differentiating Eq. (3) with respect to $\bar{v}$ and setting the result equal to zero. Then, solving for $\bar{v}$ one finds

$$\bar{v}_{opt} = \sqrt{48} D_A/R \tag{6}$$

Some workers have calculated D_A from Eq. (6) by an experimental determination of $\bar{v}_{opt}$, while others by solving Eq. (5). This latter case requires the values of $\bar{v}, \hat{H}$ and R. The R can be measured directly, whilst $\bar{v}$ can be found by dividing the length l of the tube by the retention time t_R of the solute. The value of $\hat{H}$ is found from a relation mentioned before:

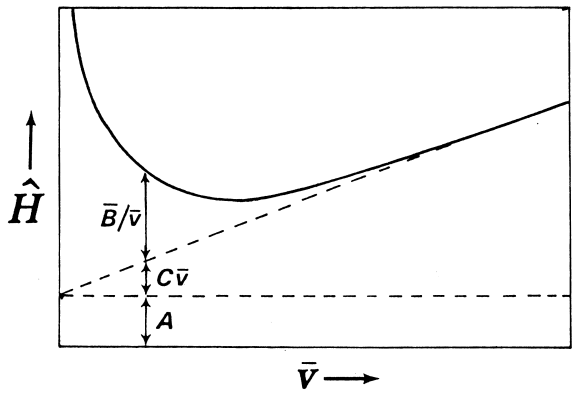

Fig. 1. Plot of Van Deemter equation (Eq. (4)), showing the contribution of the three terms A, $\bar{B}/\bar{v}$ and $C\bar{v}$ to the plate height $\hat{H}$ at a specified mean axial flow velocity $\bar{v}$.

$$\hat{H} = \frac{\sigma_x^2}{l} = \frac{(\sigma_t \bar{v})^2}{l} = \frac{\sigma_t^2 (l/t_R)^2}{l} = \frac{(W_{1/2}/2.3548)^2 l^2/t_R^2}{l} = \frac{W_{1/2}^2 l}{5.545 t_R^2} \tag{7}$$

where $W_{1/2}$ is the width of the elution peak at one-half the peak height.

2.1.2. Experimental

The most common set-up for the broadening technique is a commercial GC apparatus equipped with a coiled, long (30 m or more) empty cylindrical tube and an appropriate detector for the solute being studied (cf. Fig. 2 of Ref. [9]). Some workers have used packed columns or other experimental arrangements [9].

Various sources of error arise in the diffusion coefficient measurements by the broadening technique. First, is the effect of finite injection volume, detector volume and dead volume of the connecting tubes. Second, is the input distribution of the solute vapor. Ideally, the sample should enter the column as an infinitely narrow plug, i.e. a Dirac delta function. Since this is difficult to be approached experimental-

ly, ingenious injection devices have been built and used by several authors [10–13]. Third, temperature gradients must be kept to a minimum in the column, and a steady flow of the carrier gas is needed. The latter can be a difficult problem, since there is virtually no pressure drop across the column. Fourth, the column coiling causes secondary flow phenomena, stagnant pockets, etc.

2.1.3. Results

Maynard and Grushka in their review of 1975 [9] give a long list of diffusion coefficients of many solutes in carrier gases H_2, He, N_2, O_2, Ar, CO_2, CH_4 and CF_4, determined by broadening techniques at various temperatures and pressures. The precision and accuracy of the determination are also listed in most cases.

2.2. The stopped-flow technique

Although there would be no gas chromatography without a mobile gas phase, i.e. a carrier gas, its linear velocity u or volume flow-rate $\dot{V}$ remains constant throughout a single experiment in most gas chromatographic studies, or analytical applications. Thus, this magnitude is usually treated as an adjustable parameter of gas chromatographic equations. Following, however, the widespread use of temperature programming in gas chromatographic analysis, the programming of the carrier gas inlet pressure, and hence its flow-rate, had also been reported and reviewed [14,15]. In spite of the development of various programming modes (e.g., step programming, continuous linear and non-linear programming), and the existence of commercial units permitting the general use of the technique, flow (pressure) programming has not been used to extract information of a physicochemical nature in gas chromatography. Its uses have been limited to analytical applications.

Except for flow programming, there are two other kinds of flow-rate perturbations imposed on the carrier gas. These are the *stopped-flow* and the *reversed-flow* techniques mentioned in the Section 1. The first consists in *stopping* the carrier gas flow for short time intervals, which is most easily done by using shut-off valves. Thus, sophisticated mechanical, pneumatic or other special systems are not required as in flow programming gas chromatography.

To the best of our knowledge, the first who used the stopping of the carrier gas flow for varying time periods were Knox and McLaren [12], with the purpose of producing extra broadening of the chromatographic peaks for measuring gas diffusion coefficients. However, the stopped-flow method was substantially introduced in 1967 by Phillips and his co-workers (see Ref. [4], pp. 551–555) to study chemical reactions on the chromatographic column. This technique has solely been used for physicochemical measurements and constitutes some of the objects of Ref. [7].

2.2.1. Mathematical model

Stopped-flow gas chromatography was employed 14 years after its discovery [16], not for a mere broadening of an existing chromatographic zone, but to create new very narrow peaks (*stop peaks*) on an asymmetrical elution curve of an analyte A. The decay of these stop peaks with time was used to determine the diffusion coefficient of A into another gas B, with much shorter columns than those used in broadening techniques. The decisive column part can be made straight, so that secondary flow phenomena due to coiled tubes were avoided.

Consider a conventional tubular empty GC column, at one end of which a small volume of the pure component A is instantaneously introduced, as a gas or vapor, in the form of a pulse (by means of a syringe or a gas valve). The other component B fills the whole column but flows continuously only through a part of it, by entering, not at the point of injection of A, but at an intermediate position down the column, as shown in Fig. 2. This arrangement creates a discontinuity in the concentration gradient of A at the inlet point of B, i.e., at $z=L$ or $x=0$. This is because equality of fluxes of A through a cross-section of the column at $z=L$ requires that the flux in the z side due to diffusion be balanced by the flux in the x side due mainly to the bulk velocity of B. Once this discontinuity is established, a *short stop* in the flow of B will produce an accumulation of A at $x=0$, which after restoration of the B flow will be recorded by the detector as an extra stop peak, as shown in Fig. 3. This can be repeated giving a series of stop peaks, the height (and the area) of which

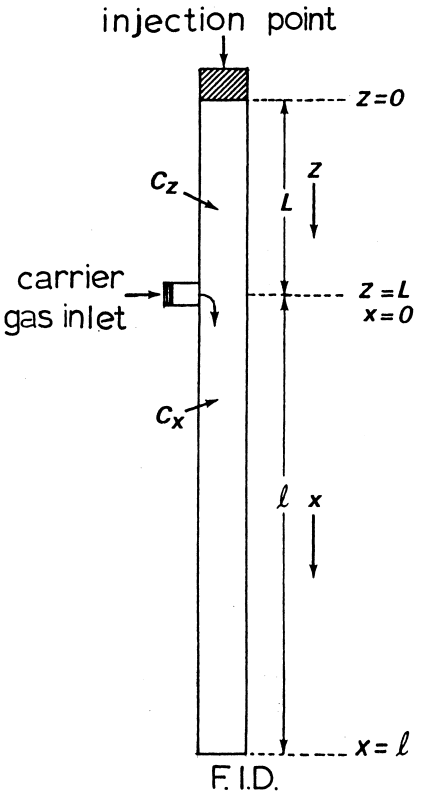

Fig. 2. Schematic representation of the diffusion column L, and the chromatographic column l for measuring binary gaseous diffusion coefficients by the stopped-flow method [16].

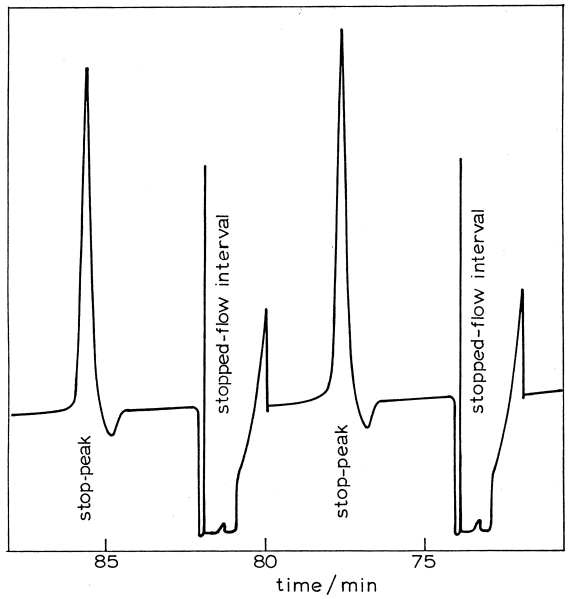

Fig. 3. A stopped-flow chromatogram showing two stop-peaks of propene in nitrogen (carrier gas) with $L=40$ cm and $l=2.7$ m [16].

diminishes with time. The problem to be solved is to determine the area under the curve of each stop peak as a function of the time of the corresponding stop in the flow of the carrier gas B.

The following assumptions are made: (a) radial diffusion in the colulmn z is negligible; (b) axial diffusion of A in the region x of the column is negligible; (c) the analyte A is introduced in an infinitesimally small section of the column region z, so that the feed band can be described by a delta function $\delta(z)$.

The time variable can be divided into three intervals, t, t_s, and t', and the problem considered separately in each of these intervals. Without going into the mathematical details which have been published [16], we can quote the milestones of the derivation. The concentration $c_z = c_z(z,t)$ is governed by the diffusion equation (Fick's second law):

$$\frac{\partial c_z}{\partial t} = D_A \frac{\partial^2 c_z}{\partial z^2} \tag{8}$$

If one compares this with Eq. (1), it is obvious why the first and third terms on the right-hand side are omitted: the first because no carrier gas B flows through section z of the column, and the third term because of assumption (a) above.

Laplace transformation of Eq. (8) with respect to t, under the initial condition

$$c_z(z,0) = \frac{m}{a_z}\delta(z) \tag{9}$$

where m is the amount of A injected and a_z the cross-sectional area in region z, leads to a linear second-order differential equation, which is solved by classical methods. The constant of integration of this solution is determined by the boundary conditions at $z=L$ or $x=0$:

$$(c_z)_{z=L} = (c_x)_{x=0} \quad \text{and}$$

$$-D_A a_z \left(\frac{\partial c_z}{\partial z}\right)_{z=L} = v a_x (c_x)_{x=0} \tag{10}$$

For $L \to \infty$, i.e. for an infinite column length before

the carrier gas inlet, inverse Laplace transformation gives the well-known result for a semi-infinite cylinder:

$$c_z = \frac{m}{a_z(\pi D_A t)^{1/2}} \exp\left(-\frac{z^2}{4D_A t}\right) \quad (11)$$

The concentration c_x under the assumption (b) obeys the mass balance equation

$$\frac{\partial c_x}{\partial t} = -v\frac{\partial c_x}{\partial x} \quad (12)$$

where v is the linear velocity of carrier gas B in column l. Using Laplace transforms of the terms of Eq. (12), under the initial condition $c_x(x,0)=0$ and the boundary condition for $(c_x)_{x=0}$ based on the previous Eq. (10), one finds for high enough flow-rates v the solution

$$c_x = \frac{mL}{\dot{V}(\pi D_A^{1/2})(t-t_M)^{3/2}} \cdot \exp\left[-\frac{L^2}{4D_A(t-t_M)}\right] \cdot u(t-t_M) \quad (13)$$

where $t_M = l/v$ is the dead time of column l, and u is the unit step function, equal to 0 for $t<t_M$ and to 1 for $t \geq t_M$. The detector signal is proportional to c_x above, so that if the signal is multiplied by $(t-t_M)^{3/2}$ and the logarithm of the product is plotted against $1/(t-t_M)$, a straight line should be obtained with slope equal to $-L^2/4D_A$. This method, however, is not very accurate, since it requires a precise value for t_M, and a negligible distortion of the break-through curve owing to longitudinal diffusion along the column length l. A more satisfactory procedure is provided by the following.

During the stopped-flow interval t_s neither Eq. (10), i.e., equality of fluxes at $x=0$, nor Eq. (12), i.e., mass balance in the column l, holds. As a result, an accumulation of the substance A with time occurs in the region $x=0$, which is described by the equation

$$\frac{\partial c_z}{\partial t_s} = -D_A\left(\frac{\partial c_z}{\partial z}\right)_{z=L}\delta(x) + D_A\left(\frac{\partial c_x}{\partial x}\right)_{x=0}\delta(x) \quad (14)$$

If the interval t_s is sufficiently small, so that the total change Δc_x during this interval is small, one can write $\partial c_x/\partial t_s \approx \Delta c_x/t_s$. After this substitution in Eq. (14) and using Laplace transforms with respect to t, one finds for high enough v

$$\Delta C_x \approx \frac{2mt_s}{a_x}\delta(x)\exp(-qL) \quad (15)$$

where ΔC_x is the Laplace transform of Δc_x and $q=(p/D_A)^{1/2}$, p being the transform parameter for t.

At the end of the stopped-flow interval, the flow of the carrier gas B through the column length l is restored, and this corresponds to a chromatographic process through an empty column on ΔC_x (x,p) of Eq. (15). In this process C_x is taken as the baseline, on which ΔC_x 'sits'. The mass balance equation is analogous to Eq. (12), namely

$$\frac{\partial(\Delta C_x)}{\partial t'} = -v\frac{\partial(\Delta C_x)}{\partial x} \quad (16)$$

Laplace transformation of this with respect to t' (time interval following the stop), integration with respect to x and then two successive inverse transformations gives Δc_x at $x=l$, i.e. at the detector, as

$$\Delta c_x = \frac{mt_s L}{\dot{V}(\pi D_A)^{1/2}t^{3/2}} \cdot \exp\left(-\frac{L^2}{4D_A t}\right) \cdot \delta(t'-t_M) \quad (17)$$

The right-hand side of this equation has a non-zero value only for $t'=t_M$ and thus the elution of an extra narrow peak, the stop-peak, is predicted.

The area under the curve of each stop-peak is

$$f = \int_o^\infty \Delta c_x \mathrm{d}V = \dot{V}\int_o^\infty \Delta c_x \mathrm{d}t'$$

and substituting Eq. (17) for Δc_x, noting that the range of integration includes t_M, one finds

$$f = \frac{mt_s L}{(\pi D_A^{1/2}t^{3/2}} \cdot \exp\left(-\frac{L^2}{4D_A t}\right) \quad (18)$$

From this, a linear form is obtained:

$$\ln(ft^{3/2}) = \ln\left(\frac{mt_s L}{\pi^{1/2}D_A^{1/2}}\right) - \frac{L^2}{4D_A}\cdot\frac{1}{t} \quad (19)$$

which permits the calculation of D_A from the slope $(-L^2/4D_A)$ of the $\ln(ft^{3/2})$ plot versus $1/t$.

Since the stop peaks are fairly symmetrical and have a constant half-width (cf. Fig. 3), their height

from the baseline rather than their area f can be used to plot Eq. (19). This avoids complicated integrations of the stop peaks on a baseline continuously changing in slope.

2.2.2. Experimental

The experimental set-up is a simple gas chromatograph with an appropriate detector, modified as shown in Fig. 4. Both column sections L and l are empty glass tubes, 4 mm I.D., thermostated by a glass mantle (column L) or in the chromatographic oven (column l).

2.2.3. Results

The method is exemplified by some results given in Table 1. It can be seen from this Table that the differences in the values of D_A determined with varying values of L, l and $\dot{V}$ are not at all statistically significant, and lie within the 95% fiducial limits of the mean value.

Two obvious advantages of the stopped-flow method over the broadening technique are the simplicity in both, the experimental arrangement and the calculations requiring no calibration or correction. Just measuring the area or the height of the stop peaks as a function of time and a simple linear plot of them gives $L^2/4D_A$. This, divided by $L^2/4$, leads to the diffusion coefficient. As one can see from Table 1, small column lengths L are required as compared to 30 m or longer columns in the broadening technique, while the length l here is not used in the calculations.

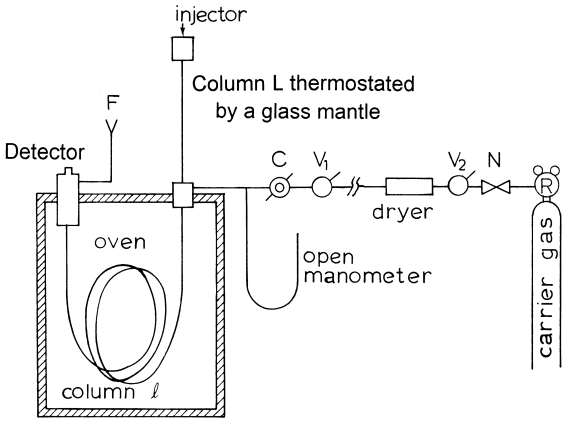

Fig. 4. Gas lines and important connections for determining diffusion coefficients by stopped-flow gas chromatography. R, two-stage reducing valve and pressure regulator; N, needle valve; V_1, V_2 = shut-off valves, for stopping and restoring carrier gas flow through column l; C, gas flow controller; F, bubble flowmeter [16].

Table 1
Diffusion coefficients of three solutes into nitrogen at 296 K and 1 atm, determined by the stopped-flow method [16]

Solute	L (cm)	l (m)	$\dot{V}$ (cm^3 s^{-1})	D (cm^2 s^{-1})
Propene	18	2.7	0.167	0.127[a]
Propene	18	2.7	0.327	0.130
Propene	18	2.7	0.833	0.129
Propene	40	2.7	0.167	0.124
Propene	18	1.5	0.167	0.124
Ethene	18	2.7	0.167	0.186[b]
Diethyl ether	18	2.7	0.167	0.0889[c]
Diethyl ether	40	2.7	0.167	0.0927

[a]Mean of seven values having a sample standard deviation of 0.003 and 95% fiducial limits of 0.127±0.0027.
[b]Literature value is 0.170 cm^2 s^{-1}.
[c]Literature value in air and 293 K is 0.089 cm^2 s^{-1}.

2.3. The reversed-flow technique

This is the second flow-rate perturbation of the carrier gas, already mentioned, avoiding sophisticated mechanical pneumatic and other special systems required in flow programming chromatography. Experimentally, it is most easily done by using a four- or six-port gas sampling valve and consists in *reversing* the direction of flow of the carrier gas, usually for a short time interval (10–100 s). Schematically, this is shown in Fig. 5.

If pure carrier gas is passing through the sampling column, nothing happens on reversing the flow. But if a solute comes out of the diffusion column at $z=0$ (cf. Fig. 5) as the result of its diffusion into the carrier gas, filling the column z and also running along the sampling column $l'+l$, the flow reversal records the concentration of the solute at the junction $x=l'$, at the moment of the reversal. This concentration recording has the form of extra chromatographic peaks (*sample peaks*) superimposed on the otherwise continuous detector signal. An example is given in Fig. 6. The peaks can be made as narrow as one wants, since the width at their half-height is equal to the duration t' of the backward flow of the carrier gas through the empty sampling column.

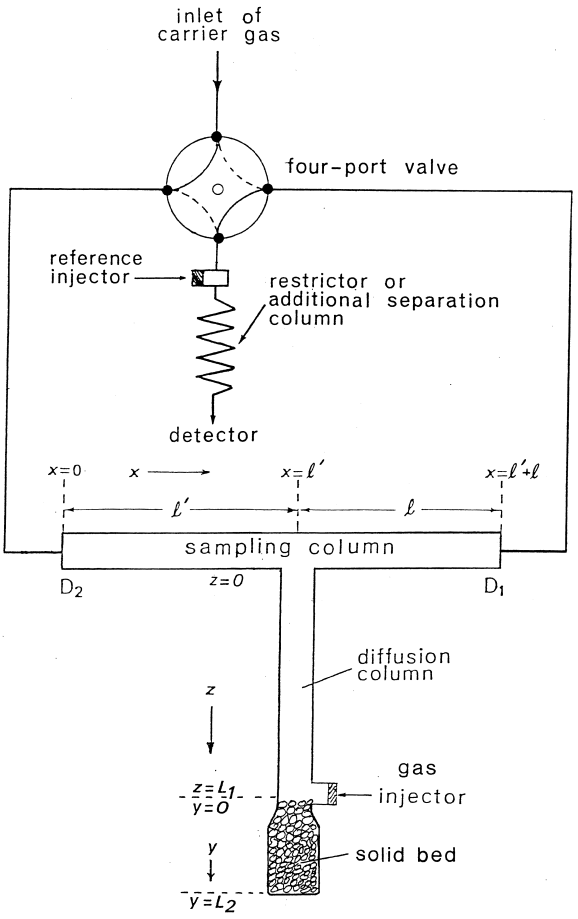

Fig. 5. Gas connections and columns in the reversed-flow technique [27].

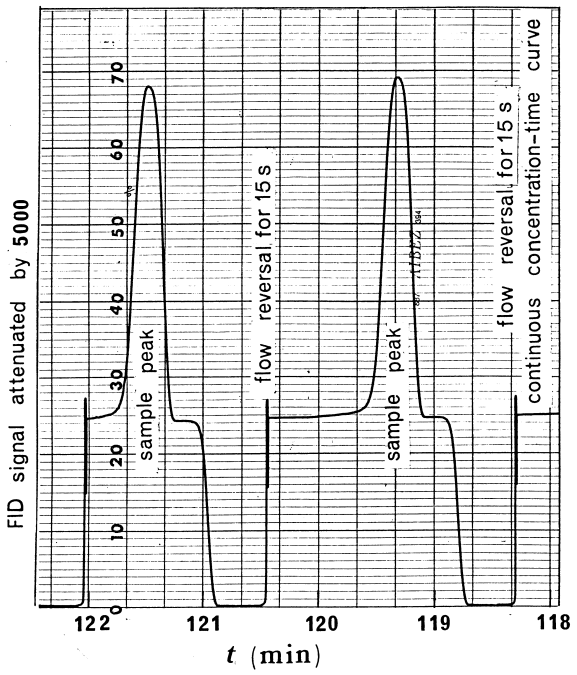

Fig. 6. A reversed-flow chromatogram with two sample peaks due to the diffusion of propene into nitrogen (carrier gas with a flow-rate of 22 cm^3/min), at 324.7 K and 1 atm (from J. Phys. Chem. 91 (1987) 3103, with permission of the American Chemical Society).

2.3.1. Mathematical models

The sample peaks are predicted theoretically by the so-called *chromatographic sampling equation*, describing the concentration–time curve of the sample peaks created by the flow reversals. It has been derived [17] using mass balances, rates of change, etc., and integrating the resulting partial differential equations under given initial and boundary conditions.

The area under the curve or the height H from the continuous signal of the sample peaks, measured as a function of the time t when flow reversal was made, is proportional to the concentration of the substance under study at the junction $x=l'$ of the sampling cell (cf. Fig. 5), at time t:

$$H^{1/M} = gc(l',t) \tag{20}$$

where M is the response factor of the detector and g a proportionality constant pertaining to the detector calibration. Measuring H experimentally as a function of t, one can construct what is termed a *diffusion band*. It is the shape and the distortion of such bands, rather than of the old elution bands that lead to the calculation of various physicochemical parameters, among which is the diffusion coefficient of gases into other gases or liquids.

In order to apply Eq. (20), the concentration $c(l',t)$ of the solute A as a function of time t is required at the junction $x=l'$ of the sampling and the diffusion columns. The simplest case for that is the determination of binary gaseous diffusion coefficients without the presence of section y in Fig. 5. Only the section z closed at $z=L_1$ is used, and the solute is injected at that point, either as an instantaneous small volume pulse or as a bigger volume to fill partly or totally the entire diffusion column L_1.

The first situation is described by Eq. (8) with initial condition described approximately by a Dirac's delta function

$$c_z(z,0) = \frac{m}{a_z}\delta(z - L_1) \tag{21}$$

L_1 being the total length of the diffusion column and the rest of the symbols having the meaning already described in connection with Eq. (9). The solution of this was first published in 1982 [18] and later [7] was more analytically given in various forms. Summarizing here, one can describe it as taking the Laplace transforms of both sides of Eq. (8) with respect to time (transform parameter p), with initial condition Eq. (21) and subject to the boundary conditions

$$c_z(0,t) = c(l',t) \quad \text{and}$$

$$D_A a_z \left(\frac{\partial c_z}{\partial z}\right)_{z=0} = \upsilon a_x c(l',t) \tag{22}$$

In the above, $c(l',t)$ is the concentration of the solute A in the sampling column at $x = l'$ and time t, $c_z(0,t)$ the concentration in the diffusion column at $z = 0$ and time t, a_z and a_x the cross-sectional areas in the columns z and x, respectively (usually taken as $a_z = a_x$), and υ the corrected linear velocity of the carrier gas in column x. The result of the above procedure is a linear second-order differential equation with respect to the t-transformed function c_z, which can be integrated by using a further double Laplace transformation with respect to z. Then, using the boundary condition $(\partial c_z/\partial z)_{z=L_1} = 0$, since there is no flux of solute across the closed boundary at $z = L_1$, and the previous boundary conditions (Eq. (22)) one obtains

$$C(l',p) = \frac{m}{a_x D_A q}\left(\sinh qL_1 + \frac{\upsilon}{D_A q}\cosh qL_1\right)^{-1} \tag{23}$$

where $C(l',p)$ is the t Laplace transformed function and $q = (p/D_A)^{1/2}$.

Inverse Laplace transformation of Eq. (23) with respect to p to find $c(l',t)$ is difficult. It can be achieved, however, by using certain approximations, the first of which is to omit $\sinh qL_1$ compared to $(\upsilon/D_A q)\cosh qL_1$, when the flow-rate is high enough so that $\upsilon/D_A q \gg 1$. Then, Eq. (23) reduces to

$$C(l',p) = m/\dot{V})\ \mathrm{sech}\ qL_1 \tag{24}$$

where $\dot{V} = a_x\upsilon$ is the volumetric flow-rate in the sampling column $l' + l$ (cf. Fig. 5). Taking now the inverse transform of Eq. (24) in the form of an elliptic theta function θ_1 [19], we obtain a summation of an infinite series of exponential functions of $1/t$ extending from $n = -\infty$ to $n = \infty$. If the first four terms around $n = 0(-1,0,1,2)$ are written explicitly, we obtain

$$c(l',t) = \frac{N_1}{t^{3/2}}\left[\exp\left(-\frac{L_1^2}{4D_A t}\right) - 3\exp\left(-\frac{9L_1^2}{4D_A t}\right)\right] \tag{25}$$

where

$$N_1 = mL_1/\dot{V}(\pi D_A)^{1/2} \tag{26}$$

By using long enough diffusion columns (say $L_1 = 80$ cm), and taking measurements at short times, one can ignore the second term inside the brackets [ ], since it contains an exponent nine times bigger than that of the first term.

Substituting Eq. (25) for $c(l',t)$ into Eq. (20) (having omitted the last term on the far right), one obtains, after rearrangement and taking logarithms,

$$\ln(H^{1/M}t^{3/2}) = \ln(gN_1) - \frac{L_1^2}{4D_A}\cdot\frac{1}{t} \tag{27}$$

Plotting the left-hand side versus $1/t$, Eq. (27) can be verified, the approximations used to derive it being assessed. The height H of the sample peaks, like those of Fig. 6, are measured from the ending baseline to the peak maximum. An example is given in Fig. 7. The diffusion coefficient is easily calculated from the slope $-L_1^2/4D_A$ of the straight line obtained and the known length of the diffusion column L_1, according to Eq. (27).

The elliptic theta function θ_1 mentioned before in the inversion of the Laplace transformation of Eq. (24) was in the form of an infinite series of exponentials of $1/t$. However, theta functions are also expressed [19] as infinite series of exponentials of t, and using this expression for θ_1, the inverse transform of Eq. (24) comes out as

$$c(l',t) = N_2\sum_{n=0}^{\infty}(-1)^n(2n+1) \times \exp[-(n+1/2)^2\pi^2 D_A t/L_1^2] \tag{28}$$

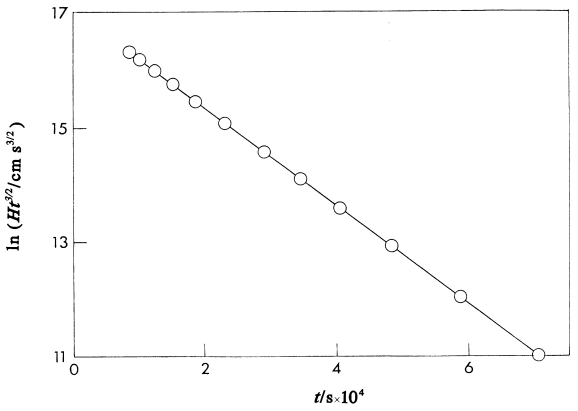

Fig. 7. Plot of Eq. (27) for the diffusion of 0.5 cm^3 C_2H_6 into N_2 at 388.5 K and 1 atm with a coiled diffusion column L of 111.4 cm×4 mm I.D. and $l'+l=99.4+99.7$ cm×4 mm I.D. [17].

where

$$N_2 = \pi\, mD_A/\dot{V}L_1^2 \tag{29}$$

If the first two terms in the summation are written explicitly, Eq. (28) reads

$$c(l',t) = N_2[\exp(-\pi^2 D_A t/4L_1^2) - 3\exp(-9\pi^2 D_A t/4L_1^2)] \tag{30}$$

This is another convenient expression for plotting experimental diffusion data, particularly for short column lengths L_1 (say 40–60 cm) and long times, since under these conditions a direct plot of $\ln(H^{1/M}) = \ln[gc(l',t)]$ versus t becomes quickly linear, after the maximum owing to the last term on the right-hand side of Eq. (30). The slope of this linear plot is equal to the exponent of the first term, $-\pi^2 D_A/4L_1^2$, from the value of which D_A is found.

The choice between Eq. (27) and Eq. (30) is a matter of preliminary experimentation with a gas of known D_A value, possibly close to that expected for the unknown D_A.

The solution of Eq. (8) with a bigger volume of solute A, introduced more slowly into the diffusion column to fill it partly or totally with the solute, is found in an analogous way as that described above for a pulse initial condition. The details for that are given elsewhere [7].

2.3.2. Experimental

The experimental set-up for the application of the reversed-flow method is particularly simple, and needs only a slight modification of a common gas chromatograph, as shown diagrammatically in Fig. 8. Any kind of GC detector can be used, although a high-sensitivity device, like a flame ionization detection (FID) system, is to be preferred. The reversing of the flow is effected by means of valve S (four-port or six-port with two alternate ports connected with a tube as shown).

While carrier gas B is flowing in the direction determined by the valve S in position indicated by the solid lines, a small amount of solute A (usually 0.5–1 cm^3 of gas at atmospheric pressure) is injected into the diffusion column L_1. After a certain time, during which no signal is noted, an asymmetric concentration–time curve of A is recorded, rising and then decaying slowly. At a certain known time (from the moment of injection) the direction of the carrier gas is reversed by switching the valve S to the other position (broken lines). After a time interval t' smaller than both the hold-up time t_R in section l and t_R' in l' of the sampling column, the initial direction of B is restored by means of the valve. This reversal of the flow direction is repeated several times, creating a whole series of sample peaks like those of Fig. 6.

The pressure drop along column $l'+l$ is negligible, and the diffusion coefficients are considered to have been determined at the pressure measured near the injection point by means of a suitable manometer.

The temperature of the diffusion column L_1 can be regulated by conventional methods. The simplest way is to coil this column and place it, together with the sampling column, inside the chromatographic oven, with its closed end at the injector position of the chromatograph.

2.3.3. Results and discussion

Two tables with the diffusion coefficient values of various hydrocarbons in carrier gases N_2, H_2 and He, determined by the reversed-flow technique at various temperatures are given in Ref. [7]. They are compared with other literature values [9] as well as with values calculated by the Hirschfelder–Bird–Spotz equation [20] or using the Fuller–Schettler–Giddings equation [21]. The first of this is given below for binary coefficients D_{AB}:

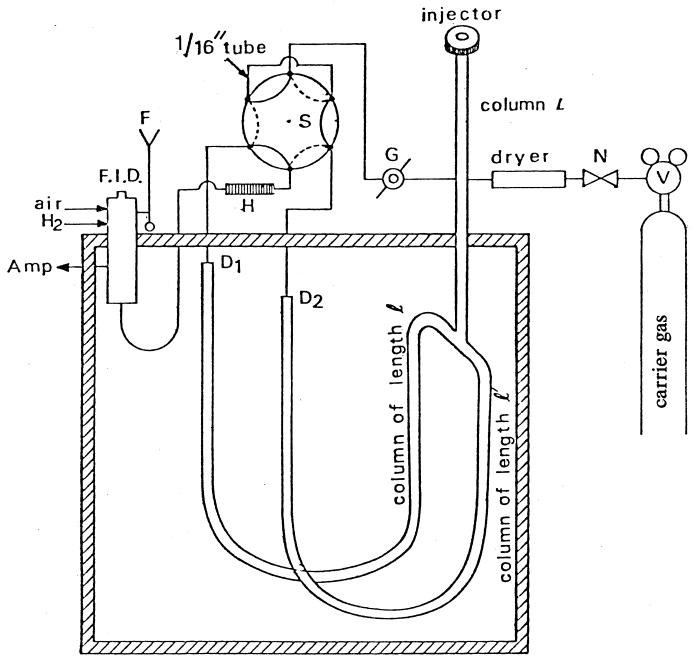

Fig. 8. Schematic arrangement of the experimental set-up for measuring gas diffusion coefficients: V, two-stage reducing valve and pressure regulator; N, needle valve; G, gas flow controller for minimizing variations in the gas flow-rate; S, six-port gas sampling valve; H, restrictor; F, bubble flowmeter; and Amp, signal to amplifier [18].

$$D_{AB} = 0.0018583T^{3/2}\left(\frac{1}{M_A}+\frac{1}{M_B}\right)^{1/2}/p\sigma_{AB}^2\Omega_{D,AB} \quad (31)$$

where M_A and M_B are molar masses, p is the pressure and $\Omega_{D,AB}$ is a dimensionless function of the temperature and of the intermolecular potential field for one A and one B molecule. Combining the Lennard–Jones parameters σ and ϵ/k of A and B, as given in Table B-1 of Ref. [20], σ_{AB} and ϵ_{AB}/k are found:

$$\sigma_{AB} = (\sigma_A + \sigma_B)/2 \quad \text{and} \quad \frac{\epsilon_{AB}}{k} = \left(\frac{\epsilon_A}{k}\cdot\frac{\epsilon_B}{k}\right)^{1/2}$$

From this, kT/ϵ_{AB} is calculated and then Table B-2 of Ref. [20] gives the $\Omega_{D,AB}$ value.

Marrero and Luecke [22] have recently modified the Fuller–Schettler–Giddings equation [21] to account for the contribution to the so-called diffusion volumes v_i of certain functional groups, like $-CH_2-$, –CO–, and –OH, particularly in long-chain alkanes, alcohols, esters and acids.

The precision of the reversed-flow method, defined either as the relative standard deviation (%) or as the relative standard error (%) associated with each value, is better than 1%, in all but three values, being 1.5, 1.2 and 2.2% [7].

Comparison of the diffusion coefficients found with those calculated theoretically, permits the calculation of the method's accuracy defined as

$$\text{Accuracy (\%)} = \frac{D_{found} - D_{calcd}}{D_{found}} \cdot 100 \quad (32)$$

With the exception of two pairs containing methane as solute, and three values for the pair C_2H_4/He the accuracy is better than 7.5% in 55 cases [7]. The high deviation of the experimental from the calculated values in the methane-containing pairs is probably due to the approximations used in the calculated values. Also, it must be noted that the Fuller–Schettler–Giddings equation [21] gives values closer to those found experimentally than other theoretical equations. Finally, the accuracies of the present method can be compared with those of the values determined by broadening techniques [9].

This comparison leads to the conclusion that with the exception of C_2H_4/N_2 the values of diffusion coefficients determined by the reversed-flow method are closer to the theoretically calculated values than are the experimental values found by broadening techniques under similar conditions of temperature and pressure.

By plotting ln D versus ln T, the exponent n in the relationship

$$D = AT^n \tag{33}$$

was calculated. For carrier gases helium and nitrogen, a mean value of 1.61 ± 0.01 and 1.74 ± 0.02, respectively, was found [17]. The mean values of n found from similar plots of calculated diffusion coefficients [20] are 1.679 ± 0.001 and 1.808 ± 0.004 for helium and nitrogen, respectively. The mean values for n, from diffusion coefficients determined by the present method, lie between the 1.5, suggested by the Stefan–Maxwell, Gilliland and Arnold equations [23] and 1.81 predicted by the Chen–Othmer equation [23]. A value of 1.75 is also predicted by the Huang [9] and the Fuller–Schettler–Giddings equation [21].

The reversed-flow method for measuring gas diffusion coefficients can be extended to simultaneous determination of diffusion coefficients in multicomponent gas mixtures [24], an experimental problem which has practical as well as theoretical importance. This extension of the method is done by filling part or all of the sampling column with a chromatographic material, e.g., silica gel, which can effect the separation of some or all components of the gas mixture. When the chromatographic sampling is then performed, preferably by having $t' < t_R$ and $t' < t'_R$, two or more sample peaks appear in the chromatogram. These correspond to two or more different components of the mixture, provided that the components have sufficiently different retention values in the filled sampling column. For each of the components Eq. (27) and Eq. (30) hold true, and therefore the maximum height, H, of each peak, measured from the ending baseline, can be plotted in the form ln $(H^{1/M}t^{3/2})$ versus $1/t$ or ln $(H^{1/M})$ versus t to yield from the slope the effective binary diffusion coefficients in the mixture. Reference [7] lists some results found [24] for ternary mixtures (a carrier gas and two hydrocarbons), together with the theoretically calculated values [20] for the diffusion of each hydrocarbon in pure carrier gas. A comparison between the experimental and the calculated values shows a difference ranging from 0.3 to 7.9%, with one exception (n-C_4H_{10} in N_2), being in that case 16%. These differences are of about the same magnitude as the accuracies for the diffusion of the same hydrocarbons in pure carrier gases.

These findings are in accord with a limiting case of the Stefan–Maxwell equations [20] which predict that for small mole fraction of components A and B in nearly pure carrier gas, the effective diffusion coefficient in the ternary mixture is equal to the diffusion coefficient of each component in pure carrier gas.

The presence of chromatographic material in the sampling column does not seem to influence the results, as shown by the binary mixture $H_2+C_2H_6$. The D value found not only coincides with the theoretically calculated value, but also is not significantly different from the value found with the sampling column empty.

2.4. Gas chromatographic methods with packed columns

The work described so far has been done with open tubes and conventional or slightly modified apparatus. Arnikar et al. [25,26] have used packed columns and an electrodeless discharge detector. They used the Van Deemter equation (Eq. (4)) to calculate the diffusion coefficient with very low carrier gas velocities, in which Eq. (4) can be approximated by

$$\hat{H} = A + \frac{2\gamma D_A}{\bar{v}} \tag{34}$$

where γ is the obstruction factor. This is usually found from the apparent diffusion coefficient γD_A by assuming a theoretical value for D_A, but the above workers assumed that $\gamma=1$ for their columns. Then, a plot of $\hat{H}$ vs. $1/\bar{v}$ yields a straight line with a slope of $2D_A$.

The arrested elution method of Knox and McLaren [12], mentioned in Section 2.2 as a stopped-flow technique, is based on extra broadening of the chromatographic peaks produced by arresting the

flow for time t. The equation describing the variance added to the peak during the delay time t is

$$\frac{d\tau^2}{dt} = \frac{2\gamma D_A}{\bar{v}^2} \quad (35)$$

where $\tau = \sigma_x/\bar{v}$. This equation is applied on both, open columns ($\gamma = 1$) and packed columns ($\gamma \neq 1$). The experiment is repeated with the same velocity $\bar{v}$, and different delay times t. The total variance is then plotted against t, yielding a straight line, whose slope is $2D_A/\bar{v}^2$. From this, D_A is calculated. If the experiment is repeated with a packed column, γD_A is found, and then γ is calculated by a simple division.

Obviously, the arrested elution method bypasses some of the experimental and theoretical difficulties of the standard continuous elution method. For example, band broadening due to flow irregularities is held constant throughout the experiment and is effectively cancelled out. Also, the column can be fairly short. However, the method still relies heavily on the time of passage of the solute along the column and the accurate measurement of the outlet elution velocity, allowing for the instrumental spreading of the chromatographic band outside the column, and other disadvantages inherent in operation at low flow-rates.

The RF-GC (reversed-flow gas chromatography) technique described in Section 2.3 does not have any of the disadvantages connected with the carrier gas flow and the instrumental spreading of the chromatographic bands, because the phenomena being studied are taking place inside the diffusion column L_1 and the vessel L_2 (cf. Fig. 5). No carrier gas flows through these vessels. The gas flows only through the column $l' + l$, and is merely used as a means for repeated sampling of the concentrations at the point $x = l'$, i.e., at the exit of the column L_1. This is done with the help of the narrow and symmetrical sample peaks mentioned before (cf. Fig. 6), without measuring their elution velocity, or the carrier gas flow-rate, provided it is steady. The experimental data recorded are the height H of the sample peaks in arbitrary units and the time t elapsing between the solute injection and the respective flow reversal, the duration of the latter being always the same (say 30 s). If one plots H or $H^{1/M}$ or $(\ln H)/M$ against t a diffusion band is obtained. An obvious difference between the old elution gas chromatography and the RF-GC is that in the former longitudinal gaseous diffusion currents are parallel with the chromatographic current and the diffusion coefficients D_A or γD_A are extracted from this mixed current by mathematical analysis. In the second method, the diffusion current is, from the outset, physically separated from the chromatogaphic current, and this is done by placing the diffusion process perpendicular to the chromatographic process. A *diffusion band*, rather than an elution band, is now mathematically analyzed to yield diffusion coefficients, or other physicochemical parameters from its distortion, in the same way that a distorted elution chromatographic band permits similar calculations. It must be pointed out that instrumental or other spreading of the sample peaks does not influence the results, as this is the same in all peaks of the same run. If the duration of the flow reversals is changed, the above spreading changes, but the physicochemical quantity extracted from the diffusion band comes out the same, provided that the same duration is maintained in all flow reversals in the same experiment.

For the simplest case of experimental set-up, i.e. when only the diffusion column L_1 exists (cf. Fig. 5) and it is not filled with any solid or liquid material, the diffusion band is described either by Eq. (25) or by Eq. (30). For a packed column or for the more general situation like that shown in Fig. 5, provided that the injected gaseous solute does not interact in anyway with the solid or liquid material filling column L_1 and/or vessel L_2, the diffusion band has been derived [27] for three cases: (a) when both, column L_1 and vessel L_2, are empty of any solid or liquid material; (b) when both, column L_1 and vessel L_2, are packed with a solid material that does not interact with the injected solute; (c) when L_1 is empty and only L_2 is packed with the above solid.

Case (c) gives a general solution comprising (a) and (b) as special cases. This solution is

$$c(l',t) = N_3\left[\frac{(Ar_1-1)(r_1-1)}{(r_1-r_2)(r_1-r_3)}\exp(-r_1\beta t) + \frac{(Ar_2-1)(r_2-1)}{(r_2-r_1)(r_2-r_3)}\exp(-r_2\beta t) + \frac{(Ar_3-1)(r_3-1)}{(r_3-r_1)(r_3-r_2)}\exp(-r_3\beta t)\right] \quad (36)$$

where

$$N_3 = \frac{m\beta}{\dot{V}A(1.29 + 1.87R)} \quad (37)$$

m is the amount of solute injected at $z = L_1$, A is given by the relation

$$A = 4L_2^2/L_1^2\gamma \quad (38)$$

R is the ratio of the gaseous volumes of vessel $L_2(V'_G)$ and column $L_1(V_G)$:

$$R = V'_G/V_G \quad (39)$$

β is the diffusion parameter:

$$\beta = \pi^2 D_A/L_1^2 \quad (40)$$

and $-r_1$, $-r_2$ and $-r_3$ are the roots of the equation

$$A(1.29 + 1.87R)\lambda^3 + (1.29 + 4.29A + \pi^2 R + 1.87AR)\lambda^2 + (4.29 + A + \pi^2 R)\lambda + 1 = 0 \quad (41)$$

when solved for λ.

If the right-hand side of Eq. (36) is substituted for $c(l',t)$ in Eq. (20), the height H of the sample peaks as a function of time is obtained, i.e. the function describing the diffusion bands (cf. Fig. 9), when the column L_1 is empty and the vessel L_2 is packed with a solid not interacting with the injected solute.

Eq. (36) also describes the diffusion band when column L_1 and vessel L_2 are both empty of any solid material or both packed with non-reacting material. In these two cases, however, $A = 4L_2^2/L_1^2$ and the parameter R will have the same value irrespective of whether L_1 and L_2 are both empty or both packed with solid. Therefore, the values of A and R are in these cases characteristic of the cell dimensions, and with the help of them the roots $-r_1$, $-r_2$ and $-r_3$ of Eq. (41) can be found with any desired precision. These roots differ considerably from one another, making the exponential coefficients $-r_1\beta$, $-r_2\beta$ and $-r_3\beta$ of the three functions in Eq. (36) very different, and therefore easily determinable from the experimental diffusion band. For example, the absolutely smaller root, say $-r_3$, describes the diffusion band at long enough times, i.e., after its maximum (cf. Fig. 9), when the other two exponential functions have already decayed to negligibly low values. It corresponds to the last linear part of the band, when the latter is a semilogarithmic plot. The slope of this part gives $-r_3\beta$ and, using Eq. (40), the diffusion coefficient D_A of the solute in the carrier gas is easily calculated.

2.4.1. Two limiting cases of Eq. (36)

The first arises when $L_2 = 0$ and $V'_G = 0$, i.e., the vessel L_2 is absent. Then, $A = 0$ and $R = 0$, Eq. (41)

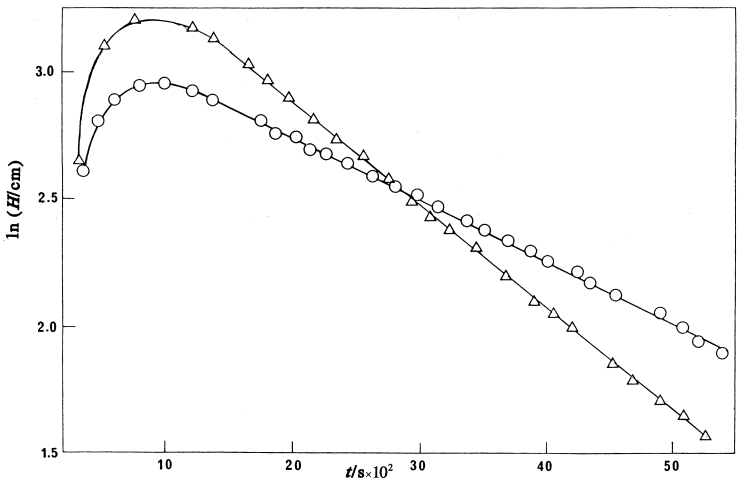

Fig. 9. Diffusion bands obtained at 313.2 K with a thermal conductivity detector, using helium as carrier gas and nitrogen as solute; ○, vessel L_2 empty; △, vessel L_2 filled with glass beads of diameter 3 mm [27].

reduces to $1.29\lambda^2+4.29\lambda+1=0$, with roots $-r_1=-3.073$ and $-r_2=-0.2522$, and Eq. (36) becomes

$$c(l',t)=\frac{m\beta}{\dot{V}}[0.2055\exp(-0.2522\beta t)+0.5697\exp(-3.073\beta t)] \quad (42)$$

which almost coincides with Eq. (30) with small differences in the numerical coefficients. Therefore, the slope of the last linear part is $-0.2522\beta=-0.2522\pi^2 D_A/L_1^2=-\pi^2 D_A/3.97L_1^2$, which coincides with that predicted by Eq. (30).

The second limiting case of Eq. (36) is obtained when $L_2 \ll L_1$ and thus A can be set equal to zero. In that case only the volume ratio $R=V'_G/V_G$ determines the roots of Eq. (41) which reduces to

$$(1.29+\pi^2 R)\lambda^2+(4.29+\pi^2 R)\lambda+1=0 \quad (43)$$

If these roots are $-r_1$ and $-r_2$, the following expression is obtained instead of Eq. (36):

$$c(l',t)=N_4\left[\frac{r_1-1}{r_1-r_2}\exp(-r_1\beta t)+\frac{r_2-1}{r_2-r_1}\exp(-r_2\beta t)\right] \quad (44)$$

where

$$N_4=\frac{m\beta}{\dot{V}(1.29+\pi^2 R)} \quad (45)$$

2.4.2. Measurement of gas diffusion coefficients

Injecting a small gaseous volume (0.5–1 cm^3 at atmospheric pressure) of a solute at the lower end of the diffusion column (cf. Fig. 5), and then performing repeated flow reversals for 10–60 s, we obtain a series of sample peaks. The height H of these peaks from the ending baseline are plotted as $(1/M)\ln H$ vs. the time of each reversal t measured from the injection moment, when a diffusion band is obtained (cf. Fig. 9). The slope of the last linear part of this plot gives the diffusion coefficient D_A of the injected solute into the carrier gas:

$$\text{Slope}=-r_2\beta=-r_2\pi^2 D_A/L_1^2 \quad (46)$$

where $-r_2$ is the absolutely smallest root of Eq. (43) when both L_1 and L_2 are empty of solids and $L_2 \ll L_1$ or $-r_2=-0.2522$ if vessel L_2 is absent.

2.4.3. Determination of the obstruction factor γ

This factor is defined by Giddings [23] and also stressed by Knox and McLaren [12] as arising from two effects, namely, the tortuosity of the paths through the medium and the alternating constriction and widening of the paths. Two experimental plots at the same temperature, using the same cell, are required for this determination: (a) a diffusion band with both the diffusion column L_1 and the vessel L_2 empty of any solid, and (b) a diffusion band with both L_1 and L_2 packed with the solid material under study, provided that a gaseous solute, that is not sorbed by the solid or does not interact with it in any way, is used in the diffusion experiment. If the slopes of the last linear parts after the maximum of the above bands are b(empty) and b(packed), their ratio gives directly the value of the obstruction factor, without any other measurement or correction:

$$\frac{b(\text{packed})}{b(\text{empty})}=\frac{-r_2\beta(\text{packed})}{-r_2\beta(\text{empty})}=\frac{\pi^2\gamma D_A/L_1^2}{\pi^2 D_A/L_1^2}=\gamma \quad (47)$$

This relation is based on the fact that the parameters A and R have the same value in both experiments (a) and (b) described above. Therefore, all roots $-r_1$, $-r_2$ and $-r_3$ of Eq. (36) are the same whether the cell is empty or packed. The root $-r_2$ is taken as having the smaller value, and thus describing the last linear part of the diffusion band. The value of the diffusion parameter β is given by Eq. (40), with the diffusion coefficient being D_A when the cell is empty, and γD_A when it is packed.

It must be noted that the simpler functions described by Eq. (42) and Eq. (44) lead to exactly the same Eq. (47). This means that the experiments could be conducted only with column L_1, without the presence of vessel L_2, although in this case only the obstruction factor, but not the porosity of the solid bed, could be determined, as shown below.

2.4.4. Determination of the external porosity ϵ

One more diffusion band, in addition to those described under (a) and (b) above, is required for this determination: (c) a band obtained with the diffusion column L_1 empty and vessel L_2 packed with the solid under study. This is the case leading to the most general solution, i.e., Eq. (36). The slope of the last

linear part of the band, b(semi-packed), is now required. The steps to be taken for calculating the porosity are to find the experimental slopes b(empty) and b(semi-packed), the lengths L_1 and L_2, the volumes V'_G(empty) and V_G, and the value of γ from the previous determination. Using the values of $A(\text{empty}) = 4L_2^2/L_1^2$ and $R(\text{empty}) = V'_G(\text{empty})/V_G$ in Eq. (41), its roots are found, the absolutely smaller one $-r_3$ being retained. Then, using the relation

$$\frac{b(\text{semi-packed})}{b(\text{empty})} = \frac{-r_{3s}\beta}{-r_3\beta} = \frac{-r_{3s}}{-r_3} \tag{48}$$

$-r_{3s}$ is computed. This is used, together with the new value of $A(\text{semi-packed}) = 4L_2^2/L_1^2\gamma$, to find R(semi-packed) by the relation

$$R(\text{semi-packed}) = \frac{1.29Ar_{3s}^3 - (1.29 + 4.29A)r_{3s}^2 + (4.29 + A)r_{3s} - 1}{-1.87Ar_{3s}^3 + (\pi^2 + 1.87A)r_{3s}^2 - \pi^2 r_{3s}} \tag{49}$$

Finally, the porosity ϵ is calculated from the ratio

$$\epsilon = \frac{R(\text{semi-packed})}{R(\text{empty})} = \frac{V'_G(\text{packed})}{V'_G(\text{empty})} \tag{50}$$

More details and results obtained by this method can be found in the original paper [27].

3. Diffusion of gases in liquids

Unlike diffusion coefficients in gases, open gas chromatographic columns cannot be used for diffusion coefficients in liquids. Either packed and capillary columns, or RF-GC arrangements are necessary.

3.1. Packed column broadening method

As mentioned in the respective Section 2.1 for diffusion in gases, the Van Deemter equation (Eq. (4)) describes the peak broadening. The second and the third terms $\bar{B}/\bar{v} + C\bar{v}$ of this equation have the form of Eq. (3), which is based on the Gaussian variance σ_x^2 in the limit of a long column as given by Eq. (2). However, in a packed column the total broadening measured again by the total variance in length units, is obtained by adding the following two equations:

$$\sigma_{1x}^2 = 2D_G t\gamma = \frac{2D_G l\gamma}{\bar{v}} \tag{51}$$

$$\sigma_{2x}^2 = \frac{8}{\pi^2} \cdot \frac{d^2\bar{v}}{D_s} \cdot \frac{kl}{(1+k)^2} \tag{52}$$

where D_G = diffusion coefficient of the solute into the carrier gas due to longitudinal diffusion in the gas phase; k = partition ratio of the solute in the packed column; d = thickness of the liquid layer on the solid support in GL chromatography, or depth of pores of uniform bore in GS chromatography; D_s = diffusion coefficient of the solute in the stationary phase.

The other symbols t, γ, $\bar{v}$ and l have the same meaning as before, i.e., time elapsing from the pulse injection of solute, obstruction factor, mean axial flow velocity, and column length, respectively.

The first equation relating to the coefficient $\bar{B}$ of Eq. (4) is Einstein's law of longitudinal diffusion in the gas phase ($\sigma_x^2 = 2D_G t$), multiplied by the obstruction factor γ to account for the fact that diffusion is not exactly along the chromatographic column axis, but along the tortuous paths between the particles of the packing.

The second equation pertaining to the coefficient C of Van Deemter equation, is due to the non-instantaneous equilibration of solute between the two phases. This is the most common mechanism among those tabulated by Giddings ([23], p. 190) to account for the value of the C term.

If Eq. (51) and Eq. (52) are added and the resulting σ_{total}^2 divided by l, the plate height $\hat{H}$ of the column is obtained as a function of the mean linear velocity $\bar{v}$, i.e., Van Deemter equation:

$$\hat{H} = A + \frac{2D_G\gamma}{\bar{v}} + \frac{8}{\pi^2} \cdot \frac{d^2}{D_s} \cdot \frac{k}{(1+k)^2}\bar{v} \tag{53}$$

The term A is added to account for flow independent contributions to $\hat{H}$. The derivation of Eq. (51) and Eq. (52) are given in detail elsewhere (Ref. [7], pp. 18–28). The separate terms A, $\bar{B}/\bar{v}$ and $C\bar{v}$ of Eq. (53) are calculated on the basis of the analysis shown in Fig. 1. From the value of $C\bar{v}$, d^2/D_s is found according to Eq. (53), but the problem is the

calculation of d. This is very difficult to do accurately for packed columns, since the liquid phase is spread on porous supports in a complex way, though a method to determine an average film thickness is available (Ref. [4], p. 472). The situation for capillary columns is somewhat simpler to handle. With glass beads columns the film may be more uniform, permitting a more satisfactory evaluation of an average d. An alternative way is to calculate ratios of D_s, since the d values can be arranged to cancel. Or, if D_s is known for one solute in one stationary phase, it is possible to estimate d for that stationary phase and hence D_s of any other solute in that stationary phase.

3.2. Other studies on band broadening

Some unbiased measurement methods of peak attributes – mainly their statistical moments and cumulants – were developed to exploit diffusion-controlled band broadening phenomena in chromatography and for studying transport processes in porous solids. In addition to numerical integration and fitting methods for determining peak shape attributes, a method based on the use of Edgworth–Cramér series expansion was proposed and validated [28–32]. This series expansion is in fact not only a 'flexible' function, but it also has a basic role in approximating Gaussian-type processes like chromatography, since it is directly connected to the Central Limit Theorem of the Probability Theory (in practice it is an expansion related to this theorem) [29,31,32]. The method was compared to the numerical integration method and to the use of different fitting functions such as the Gram–Charlier expansion [28–30] and it was discussed from a basic point of view [31,32] in the context of the stochastic theory of chromatography.

The Edgworth–Cramér peak shape fitting method was applied to exploit the transport properties of active carbons [33] and to evaluate the chromatographic performances of high-speed chromatography [34]. This last work is one of the rare examples of both high-precision evaluation and validation of Van Deemter plots in high-speed high-precision chromatography for an unretained component. Instead of Eq. (34), the HETP expression employed for packed columns is

$$\hat{H} = \left(2\lambda d_p + \frac{2\gamma D_{og}}{v_o}\right)\frac{9(P^4-1)(P^2-1)}{8(P^3-1)^2} \qquad (54)$$

where P is the ratio between the inlet and the outlet pressures, P_i and P_o, respectively, v_o the outlet gas velocity, D_{og} is the solute gas diffusion coefficient at the column outlet pressure, d_p the packing particle diameter, and λ a constant.

3.3. Reversed-flow method

The experimental arrangement to measure diffusion coefficients of gaseous solutes into liquids is that of Fig. 5, with vessel L_2 filled with the pure liquid under study in place of the solid bed, and the solute injected as a pulse (0.5–1 cm^3 at atmospheric pressure) at the lower part ($z = L_1$) of the diffusion column. The experiment is conducted in exactly the same way as that described in the determination of diffusion coefficient in gases (Section 2.3), giving rise to a diffusion band like those of Fig. 9.

3.3.1. Mathematical model

The function describing the diffusion band in this case, with a quiescent liquid, has been derived [35] by the following steps. The diffusion Eq. (8) is written for the gas phase in region z (cf. Fig. 5) under the initial condition (Eq. (21)), the boundary conditions at $z = 0$, i.e., Eq. (22), where the carrier gas is passing in the x direction, i.e., perpendicularly to the direction of the gaseous diffusion. Then, the diffusion Eq. (8) is written for the liquid phase in region y:

$$\frac{\partial c_y}{\partial t} = D_L \frac{\partial^2 c_y}{\partial y^2} \qquad (8a)$$

The solution of the equations in regions z and y are linked using the boundary conditions at $z = L_1$ and $y = 0$. The final equation, obtained under certain approximations [35], gives the concentration $c(l',t)$ of the injected solute at the junction $x = l'$ (cf. Fig. 5) and at time t. This, combined with Eq. (20), gives the height H of the sample peaks as a function of time:

$$H^{1/M} = N_5\left[\left(1+\frac{Z}{Y}\right)\exp\left(-\frac{X+Y}{2}t\right) + \left(1-\frac{Z}{Y}\right)\exp\left(-\frac{X-Y}{2}t\right)\right] \quad (55)$$

where

$$N_5 = \frac{3gmD_G}{2\dot{V}L_1^2(1+3V'_G/V_G)} \quad (56)$$

$$X = \frac{3\beta + 72K\alpha V_L/V_G}{\pi^2(1+3V'_G/V_G)} + 25\alpha \quad (57)$$

$$\frac{X^2-Y^2}{4} = \frac{75\alpha(\beta+16K\alpha V_L/V_G)}{\pi^2(1+3V'_G/V_G)} \quad (58)$$

$$Z = X - 50\alpha \quad (59)$$

and g = calibration factor for the detector; m = amount of solute injected; $\dot{V}$ = volumetric flow-rate of the carrier gas; V'_G = gaseous volume in L_2 above the liquid; V_G = gaseous volume in the diffusion column L_1; V_L = volume of the liquid in vessel L_2; K = partition coefficient of the solute between the liquid and the carrier gas; α,β = diffusion parameters given by the relations $\alpha = \pi^2 D_L/4L_2^2$ and $\beta = \pi^2 D_G/L_1^2$, D_L and D_G being the diffusion coefficient of the solute gas into the liquid and the carrier gas, respectively.

Eq. (55) describes the descending branch of the diffusion band as a sum of two exponential functions. The exponential coefficients $(X+Y)/2$ and $(X-Y)/2$, together with the respective pre-exponential factors, can be determined by means of a non-linear regression analysis computer programme (Ref. [36], Appendix A). There are two ways to calculate D_L and K (or the Henry's law constant) from the diffusion band: either by using the two exponential coefficients $(X+Y)/2$ and $(X-Y)/2$, and the diffusion parameter β, or by employing the above exponential coefficients and the respective pre-exponential factors $N_5(1+Z/Y)$ and $N_5(1-Z/Y)$ of Eq. (55), found from the intercepts, as mentioned above. In both ways the gaseous volumes V'_G and V_G, the volume of the liquid V_L and the height of the liquid L_2 are required.

According to the first way, the sum of the two exponential coefficients $(X+Y)/2$ and $(X-Y)/2$ gives the value of X, i.e., the right-hand side of Eq. (57), while their product Π equals $(X^2-Y^2)/4$, i.e., the right-hand side of Eq. (58). If Eq. (57) is solved for $K\alpha V_L/V_G$ and the result is substituted into Eq. (58), one obtains a quadratic equation in α:

$$1250\alpha^2 - 25\left[\frac{3\beta}{\pi^2(1+3V'_G/V_G)} + 2X\right]\alpha + 3\Pi = 0 \quad (60)$$

This on solution gives the value of $\alpha = \pi^2 D_L/4L_2^2$ from which D_L is computed as L_2 is a known length. The α value found is then substituted back in Eq. (57) or Eq. (58) to find K.

The second way starts again from the sum of the two exponential coefficients $(X+Y)/2$ and $(X-Y)/2$ and finds the value of X. Their difference gives the value of Y. From the ratio ρ of the two pre-exponential factors of Eq. (55):

$$\rho = \frac{1-Z/Y}{1+Z/Y}$$

one calculates the value of Z:

$$Z = \frac{1-\rho}{1+\rho}Y \quad (61)$$

The fact that arbitrary units are used for the height H of the sample peaks, from which the diffusion band is constructed, does not influence the value of Z, since it is calculated from the ratio ρ of two intercepts pertaining to the same substance and the same experiment, so that any unknown proportionality factors cancel out.

Eq. (61) combined with Eq. (59) gives the value of α as

$$\alpha = \frac{1}{50}\left(X - \frac{1-\rho}{1+\rho}Y\right) \quad (62)$$

from which D_L is found.

The value of K can now be calculated without using the value of the diffusion parameter β, by solving Eq. (57) for β and substituting it in Eq. (58). The result is

$$K = \frac{X - 25\alpha - \Pi/25\alpha}{24\alpha V_L/V_G}\pi^2(1+3V'_G/V_G) \quad (63)$$

3.3.2. Results and discussion

The method described here was applied by conducting experiments with three liquids, namely,

hexadecane, heptane and water, and two gases, namely, ethene and propene [35]. The diffusion coefficients of the gases into the liquids D_L, the partition coefficients K, and the Henry's law constants H_+(atm) were calculated by both ways mentioned above (1 atm = 101 325 Pa). It was then pointed out that there are no significant differences between the values found by using two completely different ways of calculation, which are based on different experimental data. This is an indication of the internal consistency of the theory.

The results found experimentally as described in this section can be compared with those calculated using the Wilke–Chang formula [37]:

$$D_L = 7.4 \times 10^{-8} \cdot \frac{T(xM_B)^{1/2}}{\mu_B V_A^{0.6}} \quad \text{cm}^2/\text{s} \qquad (64)$$

where M_B is the molar mass of the liquid, T the absolute temperature, μ_B the viscosity of the liquid in cp, V_A the molar volume of the solute at the normal boiling point in cm^3/mol, and x an 'association' factor. Some values of x are 2.6, 1.9, 1.5, for water, methanol and ethanol, respectively, and 1.0 for benzene, ether and heptane.

Molar volumes of complex substances can be estimated by adding up the contributions of the atoms in the molecule [37].

4. Diffusion in supercritical solvents

The distinction between GC and LC disappears just above the critical point of the carrier, the technique has been termed *supercritical fluid chromatography* (SFC). The high pressure permitted in this technique offers the possibility to measure diffusion coefficients of large molecules in supercritical or near-critical fluids. The literature diffusion data are scarce and possibly inaccurate in this area. Roth has reviewed the subject of diffusion and thermodynamic measurements by SFC [38], pointing out that the method widely used is that of the broadening technique described in Section 2.1. Eq. (3) derived there is applied. The main features of the apparatus used for such measurements are given in a previous paper by Roth et al. [39] dealing with limiting diffusion coefficients of 10 model polycyclic aromatic hydrocarbons in compressed propane at 384.4 K and 103.4 bar pressure.

5. Adsorption

Non-linear non-ideal gas-solid chromatography offers a unique means of studying thermodynamic parameters of adsorption, and adsorption isotherms at very low surface coverage, a region of concentrations very important in characterizing the structure of the solid surface. However, GC techniques can be extended to higher concentrations as well. Such physicochemical measurements have been described in detail in the two books previously mentioned [4,5], as well as in the book by Kiselev and Yashin [40]. There are a few more recent developments, however, and only these recent works will be summarized here.

5.1. Thermodynamics of adsorption by GSC

5.1.1. Mathematical models

The basic experimental parameter determined in classical gas chromatography is the net retention volume V_N, and this quantity can be expressed in terms of changes in thermodynamic functions, like enthalpy and entropy of adsorption. Assuming that the moving phase behaves as an ideal gas mixture of carrier gas and absorbate vapor at a partial pressure p(atm), one can conclude that in adsorption equilibrium the relation

$$\mu_s = \mu_G = \mu^\theta(T) + RT \ln(p/1) \qquad (65)$$

holds true [41] expressing the equality of the chemical potentials of the adsorbate in the adsorbed state μ_s and the gas phase μ_G, μ^θ being the chemical potential in the standard state of the pure solute vapor at 1 atm. Based on that equation, the change in Gibbs free energy of adsorption is $\Delta G = \mu_s - \mu^\theta(T) = RT \ln p = RT \ln(cRT) = RT \ln(qRT/K)$, where q is the amount of solute adsorbed per unit volume of adsorbent and K the adsorption equilibrium constant. Since $V_N = V_s K$, where V_s is the volume of the solid adsorbent, substituting V_N/V_s for K in the previous relation and solving for V_N, one obtains [41]

$$V_N = RTV_s q \exp\left(-\frac{\Delta G}{RT}\right) = RTn_s \exp\left(\frac{\Delta S}{R} - \frac{\Delta H}{RT}\right) \quad (66)$$

where n_s (mol) is the total amount of the solute in the adsorbed state and ΔH, ΔS the differential enthalpy and differential entropy of adsorption, respectively. By taking logarithms of both sides, Eq. (66) can be transformed into a convenient linear form:

$$\ln V_N = \ln(RTn_s) + \frac{\Delta S}{R} - \frac{\Delta H}{R} \cdot \frac{1}{T} \quad (67)$$

Thus, by determining V_N at various temperatures, one can calculate ΔH from the slope and ΔS from the intercept of the plot of $\ln V_N$ versus $1/T$, provided that the range of T is narrow enough for ΔH and ΔS to be regarded as temperature independent. The intercept is equal to $\ln(RTn_s) + \Delta S/R$, but in ordinary gas chromatography the first term is negligible and can be ignored.

An analogous way for calculating differential enthalpy and entropy of adsorption by GSC has been described by Milonjic and Copecni [42]. It is known for a long time [44] that the differential enthalpy of adsorption is related to the isosteric enthalpy of adsorption ΔH_{st} by the equation

$$\Delta H_{st} = \Delta H + RT \quad (68)$$

As a further development [41], V_N can be expressed in terms of molecular properties, with the help of statistical mechanics. Two models for the adsorbed state were chosen, the ideal localized monolayer, and the non-localized two-dimensional ideal gas. In both cases, the mean net retention volume is calculated [41] as a function of the molecular partition functions in the adsorbed state and in the gas, the total number of active sites or the total active surface area in the column, and the distribution function $f(x)$ of the difference $x = \Delta E_o$ in the zero point energy per mol between the adsorbed and the gaseous state of the solute.

A molecular statistical theory of adsorption, taking into account the high anisotropic polarizability tensor of the adsorbent, has also been developed for various hydrocarbons on graphite [43] at zero surface coverage. This anisotropic adsorption potential model carried out for methane and benzene adsorbed on the basal (0001) graphite surface predicts values which are in good agreement with the results of gas chromatographic and static adsorption measurements on graphitized carbon blacks.

5.1.2. Experimental and results

Conventional gas chromatographic instrumentation is employed in most studies of adsorption thermodynamics by GSC.

A linear dependence of ΔS on ΔH, i.e. the so-called 'thermodynamic compensation effect' has been observed in both studies cited before [41,42]. It was shown that *n*-hexane, cyclohexane and carbon tetrachloride, i.e., non-specific interacting solutes, adsorbed on thermally treated silica beads, fall on a single straight line [42]. For benzene a separate line is obtained.

For the adsorption of saturated hydrocarbons on aluminium oxide activated at four different temperatures, the compensation effect is shown in Fig. 10 [41]. All pairs of values fall on three parallel straight lines, each comprising points from two hydrocarbons, one alkane and one cycloalkane with the same number of carbon atoms.

A molecular interpretation of the linear dependence of ΔS on ΔH on the basis of a homogeneous surface does not seem possible. Assuming that the

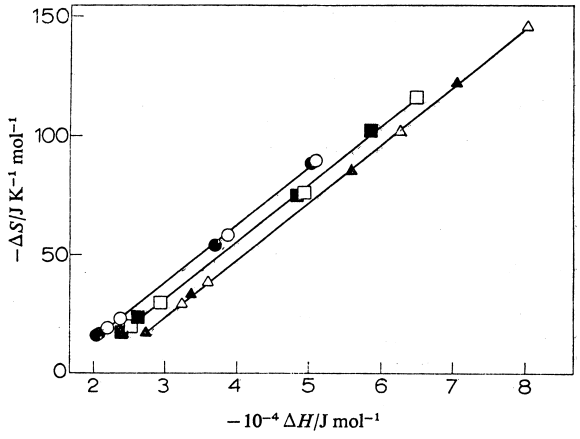

Fig. 10. Linear relationship between entropy and enthalpy of adsorption of saturated hydrocarbons on aluminium oxide; ○, pentane; ●, cyclopentane; □, hexane; ■, cyclohexane; △, heptane; ▲, cycloheptane [41].

surface is heterogeneous, we must specify the analytic form of the function $f(x)$ and the limits of integrations in calculating the mean retention volume $\langle V_N \rangle$ mentioned before, for the localized and the non-localized model [41]. As was done by Zeldowitch [45] in his classical derivation of the Freundlich isotherm, an exponential distribution of adsorption sites with respect to the energy is written

$$f(x) = a \exp\left(\frac{x}{RT_s}\right) \tag{69}$$

where a and T_s are constants for a given surface and a given type of adsorbates. The range of integration can be confined between the values x_1 and x_2 of the variable ΔE_o, such that the equilibration of the gaseous adsorbates with active sites within this range of energy is fast enough to have a significant contribution to the chromatographic variable V_N. All other adsorption sites with energy lying outside the above range are assumed to have a negligible contribution to the chromatographic process, because they equilibrate too slowly with the gas phase. It is further assumed that the activation of the surface, by heating at increasingly higher temperatures, shifts the working range of energies to more negative values by freeing or creating more energetic and faster active sites. Under these conditions, and if the range of energies between x_1 and x_2 is narrow enough, the equation giving $\langle V_N \rangle$ reads, under certain approximations

$$\langle V_N \rangle = \Phi_1 a (x_2 - x_1) \exp\left[\frac{x_1}{R}\left(\frac{1}{T_s} - \frac{1}{T}\right)\right] \tag{70}$$

where

$$\Phi_1 = \frac{h^3 q_{s_v} q_{s_{int}} nB}{(2\pi mkT)^{3/2} q_{G_{int}}} \tag{71}$$

nB is the total number of active sites in the column, and the q values denote molecular partition functions of the solute (for the vibration with respect to the surface, q_{s_v}, for internal degrees of freedom in the adsorbed state, $q_{s_{int}}$, and for internal degrees of freedom in the gas state, $q_{G_{int}}$).

Using certain approximations, we obtain $a = 1/RT_s$, and taking logarithms of both sides of Eq. (70) with $x_1 = (\Delta E_o)_1 \approx \Delta H$, we finally have

$$\ln\langle V_N \rangle = \left\{\ln\left[\frac{\Phi_1 (x_2 - x_1)}{RT_s}\right] + \frac{1}{RT_s}\Delta H\right\} - \frac{\Delta H}{R}\frac{1}{T} \tag{72}$$

This was based so far on the localized model of adsorption. For the non-localized model the same Eq. (72) is obtained, with Φ_1 having a slightly different content.

A comparison of Eq. (72) with Eq. (67) permits identification of $\ln\langle V_N \rangle$ with $\ln V_N$ and the expression in the braces $\{\}$ with $\Delta S/R$. As was noted, the first term on the right-hand side of Eq. (67) is negligible and can be ignored. Therefore,

$$\Delta S = R \ln\left[\Phi_1\left(\frac{x_2 - x_1}{RT_s}\right)\right] + \frac{1}{T_s}\Delta H \tag{73}$$

The linear dependence of ΔS on ΔH, shown in Fig. 10, is thus explained, the slope being equal to $1/T_s$. This slope should be a characteristic property of the surface, for a given family of adsorbates, a prediction fully confirmed by the experimental data [41].

The intercepts of the lines in Fig. 10 are given by $R \ln[\Phi_1 (x_2 - x_1)/RT_s]$, according to Eq. (73). These intercepts change approximately linearly with the number of carbon atoms in the adsorbate molecules. This experimental observation can be connected with a well-known empirical rule in gas chromatography, namely, the linear relationship existing between the logarithm of the retention volume (or the relative retention time) and the number of carbon atoms for the members of a homologous series, on a given adsorbent at a given temperature.

From the difference in the intercepts for hydrocarbons with $n+1$ and n carbon atoms in Fig. 10, one can calculate the frequency of the vibrations of the analyte molecules normal to the adsorbent surface.

In a further adsorption study by GSC based on the compensation effect [46], two new parameters were extracted from the experimental data. These parameters are considered to be more fundamental quantities, characterizing the adsorption phenomena rather than the enthalpy and entropy of adsorption. For the existence of a linear dependence of ΔS on ΔH, it is necessary that the straight lines predicted by Eq. (67) intersect at about the same point. At the point of intersection (defined by the pair of values

$\ln V_{N_s}$, $1/T_s$), this equation reads, neglecting the insignificant term $\ln(RTn_s)$,

$$\ln V_{N_s} \approx \frac{\Delta S_i}{R} - \frac{\Delta H_i}{R} \cdot \frac{1}{T_s} \quad (74)$$

where ΔS_i and ΔH_i refer to values calculated from line i. On rearrangement one obtains

$$\Delta S_i \approx R \ln V_{N_s} + \frac{1}{T_s} \cdot \Delta H_i \quad (75)$$

i.e., a linear dependence of ΔS_i on ΔH_i. However, it is a rather improbable situation that all lines intersect at about the same point, and the explanation that such a linear relationship exists lies on the following. For the intersection of line i with line j, Eq. (74) is

$$\ln V_{N_{i,j}} = \frac{\Delta S_i}{R} - \frac{\Delta H_i}{R} \cdot \frac{1}{T_{i,j}} \quad (76)$$

By summing over j for all $j \neq i$, we obtain

$$\sum_{j=1}^{n} \ln V_{N_{i,j}} = n\frac{\Delta S_i}{R} - \frac{\Delta H_i}{R} \sum_{j=1}^{n} \frac{1}{T_{i,j}}$$

or, on division by n and rearrangement

$$\Delta S_i = R\langle \ln V_{N_{i,j}} \rangle + \left\langle \frac{1}{T_{i,j}} \right\rangle \Delta H_i \quad (77)$$

where $\langle \ln V_{Ni,j} \rangle$ and $\langle 1/T_{i,j} \rangle$ are mean values defined by $(1/n)\Sigma_j \ln V_{N_{i,j}}$ and $(1/n)\Sigma_j(1/T_{i,j})$, respectively. Thus, for a linear dependence of ΔS_i on ΔH_i to exist, it is only necessary that the *mean values* of the coordinates of the intersection points of each line with all the rest are about the same.

The application of the above conclusion was demonstrated for the case of pentane and cyclopentane adsorbed on alumina modified with 20% (w/w) of LiCl, NaCl, RbCl, CsCl, NaF, NaBr, and NaI [46]. There were 14 plots of Eq. (67) and 91 points of intersection of these lines. The ordinates of these points range from -50.9 to 269.0, and the abscissae from -0.0137 to 0.0824, whereas the mean values of ordinates and abscissae were between 2.5 and 6.2, and between 2.3×10^{-3} and 3.6×10^{-3}, respectively. The ranges of the mean values were narrow enough to create a compensation effect according to Eq. (77).

An extended work on adsorption by GSC has been performed by Guiochon and his co-workers. Starting from superficial forces of negative charges on solid benzophenone [47], and the determination of adsorption potential of terpenes, derivatives of them and aromatic hydrocarbons on graphitized carbon black [48], they went over to theoretical studies of adsorption [49–51], and proper thermodynamics, like differential heats of adsorption and partial molar heat capacity [52], Kelvin capillary phenomena, and their influence upon the determination of adsorption coefficients [53]. Then, the general problems of calculations by statistical thermodynamics and of measurements referring to enthalpy, entropy and free energy of adsorption of vapors on graphitized carbon black [54], and measurements of the change in the heat capacity during adsorption on the same adsorbent [55] were followed by a molecular statistical theory of adsorption and prediction of the thermodynamic functions of adsorption of hydrocarbons on the above solid adsorbent [56].

5.2. Thermodynamics of adsorption by GLC

Roth et al. [57] conducted some thermodynamic studies on the retention mechanism of *n*-alkane analytes within cross-linked commercial poly(dimethylsiloxane) (PDMS) stationary phases and came to the conclusion that, although bulk dissolution appears to be the dominant retention mechanism, the relative significance of surface adsorption can be expected to increase with both the increasing size of the analyte molecule and/or the increasing degree of cross-linking of the stationary phase. In the hypothetical limit of an extremely high degree of cross-linking, a dense, three-dimensional network could be formed within the stationary film of a capillary column, preventing alkane molecules from penetrating into the bulk of the stationary phase. In such a case, the retention would be due to surface adsorption only, and the determination of thermodynamic adsorption data described in the previous subsection can be feasible. GLC is also well suited to study of adsorption at the liquid surface (Gibbs adsorption at the gas–liquid interface). Whichever process is of interest, bulk solution or liquid surface adsorption, techniques are needed to separate the two. The retention mechanisms in GLC were thoroughly interviewed by Poole and Poole [58], basing their discussion mainly on the equation

$$V_N^* = V_L K_L + A_{GL} K_{GL} + A_{LS} K_{GLS} \quad (78)$$

where V_N^* = net retention volume per gram of column packing; V_L = volume of liquid phase per gram of packing; K_L = gas–liquid partition coefficient; A_{GL} = gas–liquid interfacial area per gram of packing; K_{GL} = adsorption coefficient at the gas–liquid interface; A_{LS} = liquid–solid interfacial area per gram of packing; K_{GLS} = adsorption coefficient at the liquid–solid interface.

Eq. (78) was derived [58] from a more general equation proposed by Nikolov [59] as a general model to describe retention in GLC. Since the primary interest in using GLC to study solution behavior is to derive an accurate value for the gas–liquid partition coefficient K_L, from retention data that are independent of other concurrent retention mechanisms, Eq. (78) provides a direct approach to this goal by a simple rearrangement to

$$V_N^*/V_L = K_L + (A_{GL} K_{GL} + A_{LS} K_{GLS})(1/V_L) \quad (79)$$

A plot of V_N^*/V_L vs. $1/V_L$ will be either a curve or straight line giving K_L as the intercept at $1/V_L = 0$. The plot shape is obviously dependent on the relative importance of adsorption at the gas–liquid and gas–solid interfaces. However, in most cases a linear extrapolation to $1/V_L = 0$ can be used for finding K_L.

Eq. (78) also permits the measurement of K_{GL} if the liquid-phase surface area A_{GL} is known, e.g. from measurements by the BET method, and adsorption on the liquid–solid interface is negligible. Then, omitting the last term on the right-hand side and dividing by A_{GL}, Eq. (78) gives

$$V_N^*/A_{GL} = K_{GL} + (V_L K_L)(1/A_{GL}) \quad (80)$$

Thus, a plot of V_N^*/A_{GL} vs. $1/A_{GL}$ gives K_{GL} from the intercept and $V_L K_L$ from the slope. Since V_L is easily found, K_L can also be calculated from this plot and compared to that determined by Eq. (79).

Eq. (79) was used by Kersten and Poole [60] to calculate the values of K_L for various test probes and nine stationary phases at 80°C. From the K_L values, corrected retention index values for the test probes and McReynolds corrected phase constants were calculated and compared with the values for the uncorrected retention index and the McReynolds phase constants calculated from the adjusted retention times.

The basic Eq. (78) states that, if the various processes causing retention are independent, their contributions to the measured retention are additive. A new term $A_{GS} K_{GS}$ was added to Eq. (78) by Conder [61], describing the possibility that the liquid may not wet the support (e.g., a silanized support), so that the solute can also be adsorbed on the uncovered part of the support surface. General means of detecting adsorption contributions, identifying their type, and separating the solution and adsorption terms have also been described previously [4].

Plots of retention against loading for systems of polar solutes in hydrocarbon stationary phases on a silanized support show an unusual peak in the plot, which is believed to be due to a transition between wetting and nonwetting of the support by the liquid phase [62]. In the case of athermal solutions, the contribution of adsorption at the gas–liquid interface can be neglected.

An analysis of the relative importance of contribution of the various terms to V_N has also been given by Janák [63]. In the cases where the difference in the polarity of analyte and stationary liquid is substantial, the contribution of the term $A_{GL} K_{GL}$ increases. If the support is also inactive and has a small specific surface, the contribution of adsorption at the liquid–support interface $A_{LS} K_{GLS}$ can also be neglected, as mentioned before on deriving Eq. (80). The problem of quantitative interpretation lies in the variable surface area of the liquid A_{GL}, which can fall dramatically with increasing loading of the porous support from the surface area of the pure support coated with a monomolecular layer only, to the surface area of the geometrical surface of the support particles. It is further necessary to note that the adsorption occurring on a two-dimensional area (surface), in contrast to the absorption occurring in a three-dimensional space (solution), represents a process of discrimination for the analyte molecules. It follows, therefore, that the distribution constants change not only according to the ratio of the surface area and liquid volume, but also according to the shape and chemical function of the analyte molecule. Another variable is the competition between adsorption of the analyte molecules and the liquid on the surface of the solid support.

Some recent advances in the so-called solvation models for stationary phase characterization and the

relevant predictions of retention in GLC are worth mentioning [64,65]. The development of solvation models for GLC are based on the free energy of transfer of a solute from the gas phase to solution consisting of the additive processes of cavity formation and solute–solvent interactions, as dispersion, orientation, induction and hydrogen-bond formation. The adaptation of these models to characterize solvent selectivity for a wide range of common stationary phases and to the prediction of retention was critically discussed by Poole et al. [64]. Deficiencies in the data collections to refine solvation models for GLC led the above authors to create a new data collection in the form of gas–liquid partition coefficients corrected for interfacial adsorption. References are cited for data of more than 100 solutes on about 40 stationary phases.

In applying Eq. (78) to retention data it is assumed that the individual retention mechanisms are independent and additive, the solute concentration is in the region of the isotherm where infinite dilution and/or zero surface coverage approximations apply, and the contribution to retention from the structured liquid-phase layer in close contact with the support surface can be neglected. As described before, Eq. (79) permits the K_L values to be evaluated independently of the other contributions to retention. Also, K_{GL} can be determined by means of Eq. (80). In practice this is difficult, however, due to the lack of a straightforward and reliable experimental method for determining surface area as a function of the liquid-phase loading [66]. Insights into the importance of adsorption as a retention mechanism may also be obtained by comparing the observed experimental retention with the value calculated, assuming that the only contribution to retention was from gas–liquid partitioning. Solvation models have been proposed by Poole and co-workers, by Abraham and co-workers, and by Carr and co-workers, all three models described in detail by Poole et al. (see Ref. [64]).

A general model to characterize the individual contributions from fundamental intermolecular interactions to the gas–liquid partition coefficient K_L is the solvation parameter model developed initially by Abraham and co-workers and exploited in the same or modified form by Poole and co-workers and by Carr and Li (see Ref. [65]) to establish the solvent properties of a wide range of common stationary phases. The basis of this model is the cavity model of solvation, in which the transfer of a solute from the gas phase to solution in the stationary phase is considered to occur in three stages: (1) the creation of a cavity in the solvent of a suitable size to accommodate the solute, (2) reorganization of the solvent molecules around the cavity, and (3) introduction of the solute into the cavity where it is able to interact with the surrounding solvent molecules. The general model is based on the following equation relating K_L to the characteristic interactions for the solvation process:

$$\log K_L = c + rR_2 + s\pi_2^H + a\alpha_2^H + b\beta_2^H + l \log L^{16} \quad (81)$$

where c is a constant, R_2 the solute excess molar refraction, π_2^H the effective solute dipolarity/polarizability, α_2^H the effective solute hydrogen-bond acidity, β_2^H the effective solute hydrogen-bond basicity and L^{16} the solute gas–liquid partition coefficient on *n*-hexadecane at 25°C. The explanatory variables (R_2, π_2^H, α_2^H, β_2^H, and $\log L^{16}$) are solvation parameters derived from equilibrium measurements and are free energy-related terms characteristic of the monomeric solute. Values of the solvation parameters for more than 2000 compounds are currently available and in many cases unknown values can be estimated using simple combining rules [67,68]. The solvent properties *r*, *s*, *a*, *b*, and *l* are unambiguously defined: the *r* constant refers to the ability of a solvent to interact with solute *n*- or π-electrons; the *s* constant to the ability of solvent to take part in dipole–dipole and dipole–induced dipole interactions; the *a* constant is a measure of the hydrogen-bond basicity of the solvent; the *b* constant is a measure of the hydrogen-bond acidity of the solvent; and the *l* constant incorporates contributions from solvent cavity formation and solute–solvent dispersion interactions.

The influence of temperature on the retention mechanism and solvation interactions of 46 varied solutes in 10 representative stationary phases of different polarity within the temperature range of 60–140°C is discussed in another paper by Poole et al. [66].

Another reason affecting the course of the solute

distribution, is mass-transfer controlled by the diffusion coefficients of solutes in the gaseous and the liquid phases [63]. The first feature of this process is that the values of the rate constants differ between adsorption and desorption, the desorption velocity being the slower. Also, there is a difference of several orders of magnitude between the velocities of adsorption and absorption. As the film thickness and hence the volume of the liquid increases, not only does the absolute value of the contribution of the resistance to mass transfer increase, but also the ratio of the contribution due to absorption changes.

In principle, there are two systems: a binary gas–solid system and a ternary gas–liquid–solid system. If we consider the ternary system, it is possible to register differences in the values of the distribution constants and the differences in the rates of adsorption and desorption of an analyte on the surface of the liquid, in the bulk liquid and under the liquid on the surface of the support (liquid–solid interface).

If one considers the rate of sorption, first, diffusion of solute is controlled by coefficients D_G and D_L, where D_G is much greater than D_L. Second, it holds in general that adsorption is significantly more thermally dependent than absorption and the rate of adsorption is faster by several orders of magnitude than that of absorption.

A new method of accumulating analyte traces from a gaseous phase, like air on a liquid, can be based on the above theoretical considerations. We can imagine a liquid medium of such a chemical nature and such a surface area that adsorption becomes the mechanism controlling sorption with the different chemical structures, and partitioning properties of the analytes to be determined having relatively little effect. Details about the application of this new method for enrichment of trace amounts in gaseous phases can be found in the original publication [63].

Among the first who studied the relative importance of the dissolution and adsorption phenomena in GLC were Fontaine et al. [69], and also Vidal-Madjar et al. [70], describing the adsorption potential at the gas–liquid interface of water.

It is known [71] that retention in capillary GLC is governed by both the solute's distribution in the system gas–stationary liquid phase (SLP) and its adsorption on the interfaces of gas–SLP and SLP–solid support, i.e., the capillary inner walls (fused silica). Some authors [72–76] determined the retention of *n*-alkanes in the system gas–PEG-20M and showed that the contribution of adsorption to retention is significant, but it was not ascertained where adsorption is important, on the interface of gas–SLP or on that of SLP–solid support.

The so-called trinomial equation for the net retention volume was first proposed in 1968 [77] and has a slightly different form than Eq. (78), namely, the last term is $A_{LS}K_LK_S$, where K_S is an adsorption coefficient of the solute on the SLP–capillary walls interface. Defining $K_L = c_L/c_G$ and $K_S = c_S/c_L$, one finds by multiplication that $K_LK_S = c_S/c_G = K_{GS}$. This equation was employed by Berezkin et al. [78] to study the adsorption mechanism of C_{11}–C_{13} *n*-alkanes on open capillary columns coated with PEG-20M as SLP. They found that retention depends upon the *n*-alkanes adsorption on the gas–PEG-20M interface, but adsorption on the interface of the PEG-20M and the capillary inner wall (solid support) can be neglected. Therefore, retention was described simply by a binomial absorption–adsorption equation.

5.3. Adsorption isotherms

Adsorption isotherms by GC until 1976 were mostly determined by using frontal analysis (FA), frontal analysis by characteristic point (FACP) and elution characteristic point (ECP). The subject has been thoroughly covered since then [4,5,40]. Some newer developments, however, are worth mentioning starting by the following.

5.3.1. Step-and-pulse method

This is a fast experimental technique [79,80] achieving a constant precision in the entire pressure range in which the isotherms are determined. The problem with this method is the physical representation of the adsorption phenomenon, i.e., the correct choice of an adsorption equation, because this appears explicitly in the relationship predicting the observed retention time of a chromatographic pulse.

The step-and-pulse method combines the frontal analysis and the elution method of GC. It carries out conventional gas chromatographic measurements of retention times, using as carrier gas a mixture of an inert gas and the vapor of the compound under study.

The vapor concentration is constant during an experiment and adjusted between measurements to scan the desired range. This constant concentration mixture is the *step*. Very small *pulses* of vapor or perturbations are injected, and their retention times are observed. These perturbations can be positive or negative (vacancy), and if they are small enough the retention times will be the same.

The relation of the retention time of the pulses with the isotherm sought has been derived in detail. Here the method of calculation is outlined for a pure compound adsorption isotherm. It is based on the determination of the experimental retention $R^{E}(x_A)$ versus the mobile phase concentration x_A:

$$R^{E}(x_A) = (t_{x_A} - t_M)\frac{1}{1 - x_A}\frac{p_A^0 j_3^2}{R_g T}\frac{Q}{Sm_s} \quad (82)$$

where t_{x_A} and t_M are the pulse retention time and the dead time, respectively, x_A the mobile phase molar fraction of the solute A, p_A^o its vapor pressure, j_3^2 the pressure correction factor, R_g the gas constant, T the column temperature, S and m_s are the specific surface area and the amount of the adsorbent in the column, respectively, and Q the molar flow-rate of the inert gas. The experimental retention is fitted to a theoretically computed retention:

$$R^{T}(x_A) = \int_1^P \frac{d\alpha}{dY_A}\frac{3p^2 dp}{P^3 - 1} \quad (83)$$

where α is the amount of the solute adsorption (mol adsorbed per unit surface area), Y_A the activity of the solute in the gas phase ($=px_A/p_A^0$), P is the ratio of the input to outlet pressure (p_i/p_o) and p is the local relative pressure (measured with respect to the outlet pressure). This theoretical retention is computed, once a given theoretical model adsorption is assumed (Langmuir, Fowler and Guggenheim, Kiselev and Poshky, Virial et al.). The isotherm type selection is based on the goodness of fitting, and from the best fitting the parameters of the isotherm are determined. Thus, the method does not give directly an independent experimental isotherm. However, a significant advantage of determining the adsorption isotherm by a chromatographic method is its sensitivity to the slope of the adsorption isotherm ($d\alpha/dY_A$), and thus the ability of the chromatographic method to determine the slope with a constant precision over the whole range of the surface coverage. This feature is important in modelling the adsorption behavior.

A wonderful example for the choice of a model for the adsorption isotherm of benzene and cyclohexane on graphitized carbon black has been published [80]. Relevant in these studies was the determination of the adsorption isotherm and the determination of the lateral interaction energy of molecules in the adsorbed state by using a virial approximation for the state equation of the molecule in the adsorbed state. The step-and-pulse method, in spite of being a brilliant one, neglects the effects of longitudinal diffusion along the chromatographic column and the kinetics of mass transfer across the gas–solid or gas–liquid boundaries.

5.3.2. A chromatographic dynamic technique

This is outlined by Madey et al. in a paper dealing with adsorption interference in mixtures of adsorbate gases flowing through activated carbon adsorber beds [81] by reference to a previous work [82]. It requires a numerical integration of a time-dependent transmission curve to calculate the solid-phase concentration of the adsorbate q_o which is in equilibrium with the gas-phase concentration c_o at the bed inlet:

$$q_o(1 - \epsilon)L + \epsilon c_o L = \epsilon u c_o \int_0^\infty [1 - T(t)]dt \quad (84)$$

where ϵ = external porosity, i.e., void fraction of the adsorbing bed; L = length of the solid bed; u = interstitial flow velocity; $T(t)$ = transmission of the adsorbate given by the ratio of the adsorbate concentration $c(L)$ at the bed oulet to the concentration c_o.

The propagation time t_p is defined by the time-integral

$$t_p = \int_0^\infty (1 - T)dt \quad (85)$$

Substitution of t_p for the integral in Eq. (84) and rearrangement gives

$$\frac{\epsilon}{1 - \epsilon}\left(\frac{ut_p}{L} - 1\right) = \frac{q_o}{c_o} \equiv k \quad (86)$$

where k is the dimensionless adsorption capacity of the adsorbent for the adsorbate.

Eq. (85) is model independent and valid for any gas–solid isotherm. Single-component isotherms can be represented by the relation

$$q_o = \frac{a_o c_o^{\alpha}}{b + a_1 c_o^{\beta}} \quad (87)$$

which yields the Langmuir isotherm for $b = \alpha = \beta = 1$, and the Freundlich isotherm for $b = 0$.

5.3.3. Diffusion denuder tube method

Most of the difficulties in determining adsorption isotherms by GC arise from the presence of a carrier gas flowing through the chromatographic column. If the role of a 'gaseous carrier' of substances is confined to axial gaseous diffusion along the column holding the solid adsorbent, isotherm determination becomes much simpler with the following additional advantages compared to the older methods: the diffusion and resistance to mass transfer are not neglected, the sorption effect is non-existent, the pressure gradient is negligible along the bed, the method leads directly to an independent experimental isotherm over a wide range of concentrations, without specifying a priori an isotherm equation, and finally the isotherm can be determined in the presence of a surface reaction of the adsorbate.

This diffusion-controlled isotherm determination was published in 1995 [83] and summarized in a more recent review [84]. It will be examined again later in conjunction with catalytic studies (cf. Section 8.2).

5.3.4. Adsorption isotherm model for multicomponent interactions

A multicomponent competitive isotherm equation taking into account adsorbate–adsorbate interactions has been derived using a statistical approach [85]. The calculation assumes independence between the local configurations. The model was tested for single component adsorption. It describes satisfactorily the S-shaped isotherms observed for various gases and vapors (alkanes, nitrogen, carbon dioxide, rare gases) adsorbed on graphitized carbon black at temperatures higher than the two-dimensional critical temperature.

5.3.5. New tools in isotherms by ECP

The influence of the fluctuations of the experimental parameters on the reproducibility of the overloaded band profiles used to determine the isotherms by the ECP method was investigated using two new tools [86]. A parameter measuring the difference between two similar curves, such as overloaded elution profiles or adsorption isotherms was defined. The band profiles measured were compared with those calculated from the derived isotherm, using models from the theory of non-linear chromatography. The agreement between both profiles was defined as a distance shorter than twice the average distance between two profiles measured the same day on the same column. The degree of validity of the various assumptions made in the ECP method was assessed.

5.4. Adsorption isotherm data and surface energy distribution

Adsorption on heterogeneous surfaces has been the subject of many papers and books during the last two decades, this intensive research activity being reviewed especially in three rather recent books [87–89]. Much of the work has been devoted to evaluation of adsorption energy distribution functions by GC, usually through adsorption isotherm data. The heterogeneity effects are responsible for many interesting and important phenomena in physical adsorption, because of the predominant role of the gas–solid interactions in the majority of adsorption systems. The fundamental equation of adsorption on heterogeneous surfaces is [90]

$$q(p) = \int_a^b f(\epsilon)\theta(\epsilon, p)\mathrm{d}\epsilon \quad (88)$$

where $q(p)$ = amount of solute adsorbed at solute partial pressure p; $f(\epsilon)$ = adsorption energy distribution function; $\theta(\epsilon, p)$ = local (homogeneous) model of adsorption isotherm; ϵ = adsorption energy; a,b = limits corresponding to the minimum and maximum energy values possible.

The continuous energy distribution function is usually normalized to unity:

$$\int_a^b f(\epsilon)\mathrm{d}\epsilon = 1 \quad (89)$$

The simplest model of the localized adsorption is that of Langmuir:

$$\theta(\epsilon, p) = \frac{K(\epsilon)p}{1 + K(\epsilon)p} \tag{90}$$

where $K(\epsilon)$ is known as Langmuir's constant.

Eq. (88) is an integral equation, since the unknown function $f(\epsilon)$ appears under the sign of integration. Although the solution of such equations is a rather difficult mathematical problem in physical sciences, some simple solutions can be found by using integral transforms, like Laplace, Hilbert and Stieltjes transforms. The use of the latter in solving Eq. (88), having substituted in it Eq. (90) for $\theta(\epsilon, p)$, is described in detail by Jaroniec and Madey [88].

In 1974 Rudzinski et al. [91] applied GC data in evaluating the differential distribution of adsorption energies on heterogeneous surfaces using Hobson's method [92]. From the point of view of GC, this method is important because the data needed are directly obtained by GC, without a graphical evaluation of the adsorption isotherm in the form $V_N = V_N(p)$.

Jaroniec and his co-workers have contributed a lot to surface energy distribution functions. In 1977 they calculated the adsorption isotherms and energy-distribution functions for benzene and *n*-hexane on chemically bonded phases [93] using the mathematical model of two previous publications [94,95]. According to these, the experimental function $V_{N,t}(p)$ is approximated by the relation

$$V_{N,t}(p) = \exp\left(\sum_{i=0}^{m} B_i p^i\right) \tag{91}$$

where B_i are approximation coefficients. The parameters $\exp(B_o)$ and $B_1 RT \exp(B_o)$ characterizing the investigated systems are related to the virial coefficients and the monolayer capacity. For the purpose of calculating the pre-exponential factor of Henry's constant, K, and the average adsorption energy, $\tilde{\epsilon}$ they approximated the experimental B_o values by using the following equation [95]:

$$B_o - \ln T = \ln\left(\frac{jRN_m}{K}\right) + \frac{\tilde{\epsilon}}{R} \cdot (1/t) \tag{92}$$

where N_m is the monolayer capacity and j is the James–Martin factor. The parameters K and $\tilde{\epsilon}$ are calculated from the slopes and intercepts of the linear plot $B_o - \ln T$ versus $1/T$. Using the values of K they calculated the energy distribution function for many systems, according to the following equation [94,95]:

$$f(\epsilon) = \frac{-p^2}{F \ln 2(RT)^2}\left(\sum_{i=1}^{m} iB_i p^{i-1}\right)\exp\left(\sum_{i=0}^{m} B_i p^i\right) \tag{93}$$

where

$$\epsilon = RT \ln (K \ln 2/p) \tag{94}$$

The derivation of an integral equation describing the total net retention volume in GSC is described by Jaroniec et al. [96]. This equation has the form

$$V_{N,t}(p) = jRTn^o \int_{\epsilon_m}^{\infty} K \exp(-Kp) f(\epsilon) d\epsilon \tag{95}$$

where n^o is the total number of adsorption sites, K is the Henry's law constant, and ϵ_m the minimum adsorption energy.

Eq. (95) was transformed to another form containing the distribution of K, $G(K)$, instead of $f(\epsilon)$, with a normalization condition:

$$\int_{K_m}^{\infty} G(K) dK = 1 \tag{96}$$

the K_m associated with ϵ_m. From the several analytical functions that satisfy physical requirements, the gamma-type distribution function is the best one because it is capable of representing simple distributions with almost symmetrical, asymmetrical, or even exponential shapes. Representing $G(K)$ by a gamma distribution function, which satisfies all physical requirements, leads to a relatively simple equation for the net specific retention volume:

$$V_{N,t} = jRTn^o \exp(-K_m p)\left(\frac{q}{q+p}\right)^{m+1} \times \left[K_m + \frac{m+1}{q+p}\right] \tag{97}$$

where q and m are parameters of the gamma distribution. The details for the derivation of Eq. (97) can be found in the original publication [96].

The gamma-type distribution for the adsorption energy was also employed to model the temperature dependence of the specific retention volume for

benzene chromatographed on chemically modified porous carbon adsorbents [97,98]. The biphasic behavior in plots of $\ln V_{s,t}$ versus $1/T$ (where $V_{s,t}$ is the total specific retention volume) is interpreted in terms of differing energetic heterogeneities of the modified carbons, using the equation

$$\ln V_{s,t} = \ln(\alpha c^{o}_{s,t}) + \epsilon_m/RT - \gamma \ln(\rho RT) \quad (98)$$

where α is a temperature-independent entropy factor, $c^{o}_{s,t}$ the maximum solute surface concentration for the total surface, ϵ_m the minimum adsorption energy, γ and ρ being parameters greater than zero associated with the average adsorption energy and its dispersion. At the higher temperatures $1/\rho RT$ is nearly zero and the third term of Eq. (98) is neglected, thus creating a linear dependence of $\ln V_{s,t}$ on $1/T$. For intermediate temperatures, another approximation is made for the third term leading to another linear expression for Eq. (98):

$$\ln V_{s,t} = \ln(\alpha c^{o}_{s,t}) + \epsilon_m/RT + \epsilon^*/RT \quad (99)$$

where $\epsilon^* = \gamma/\rho$. Thus, experimental plots having the appearance of two straight lines in sequence are explained.

Hobson's method mentioned before [92] was also employed by Boudreau and Cooper [99] in their studies on determination of surface polarity by heterogeneous GSC. A slight modification of Hobson's method, used by Rudzinski et al. [91] and described before, was employed here. A form of the fundamental equation of elution chromatography including the sorption effect [4] was used. The ECP technique for determining the isotherm was employed. The conclusions of the work were that a quick, precise and sensitive technique for determining the polarity of heterogeneous surfaces has been proposed, which is applicable to a wide variety of surfaces (gels, clays, oxides, etc.), including modified ones.

A solution of the integral Eq. (88) taking into account in the local model of adsorption $\theta(\epsilon, p)$ the nearest neighbor interactions between adsorbed molecules has been reported by Jagiello et al. [100]. The local adsorption isotherm was written in the form

$$\theta(\epsilon, p) = \left[1 + \exp\frac{\epsilon_c - \epsilon}{RT}\right]^{-1} \quad (100)$$

The ϵ_c is the function called condensation energy:

$$\epsilon_c = -RT \ln\frac{p}{K} - zu\frac{V(p,T)}{V_m} \quad (101)$$

where K is the Langmuir constant, z the number of nearest neighbor adsorption sites, u the interaction energy between molecules adsorbed on two neighboring sites, V the amount adsorbed per gram of adsorbent, and V_m the monolayer capacity. The solution of the integral Eq. (88), with $V(p,T)$ in place of $q(p)$ and integration limits the minimum ϵ_1 and maximum ϵ_m values of the adsorption energy, was obtained by the so-called condensation approximation (CA) [101]. Alkane probes on silicas were used in the determinations.

From the examples of the adsorption energy distribution studies summarized above, one sees that a proper mathematical solution of the relevant integral Eq. (88) has rarely been obtained, with the only probable exception being the Sips procedure described by Jaroniec and Madey [88]. Usually approximations based on both the local adsorption isotherm $\theta(\epsilon, p)$ and the distribution function sought $f(\epsilon)$, were adopted. The latter was usually assumed a priori to obey a certain function, like the gamma function [96]. It was not obtained as a direct solution of an integral equation. Difficulties like this led scientists to turn to numerical solutions and estimations of adsorption energy distributions. Work of this kind was recently published by Guiochon and his coworkers [102–107]. In some cases comparison between analytical and numerical methods were made.

Fine, solid ceramic particles were coated on the inner wall of an open tubular quartz column. The tube was filled with a slurry of the particles under investigation in an appropriate solvent, closed at one end and introduced slowly into an oven where the solvent vaporized. Adsorption isotherms were determined by the method of ECP using large-size samples of organic vapors (diethyl ether, chlorobutane). These isotherms were then used to calculate the distribution of adsorption energy of the probe on the ceramic surface [102].

The expectation–maximization (EM) method of parameter estimation was used to calculate adsorption energy distributions of molecular probes from their adsorption isotherms [103]. EM does not require prior knowledge of the distribution function or

the isotherm, requires no smoothing of the isotherm data, and converges with high stability towards the maximum-likelihood estimate. The method is robust and accurate at high iteration numbers. The EM algorithm was tested with simulated energy distributions corresponding to unimodal Gaussian, bimodal Gaussian, Poisson distributions, and the distributions resulting from Misra isotherms. Theoretical isotherms were generated from these distributions using the Langmuir model, and then chromatographic band profiles were computed using the ideal model of chromatography. Noise was then introduced in the theoretical band profiles comparable to those observed experimentally, and the isotherm was calculated by the ECP method. The energy distribution given by the EM method was compared to the original one.

The adsorption energy distributions derived from the Adamson and Ling (AL), and the House and Jaycock HILDA numerical methods were compared with Sips analytical solution, which is used as bench mark for these numerical methods [104]. Excellent agreement between analytical and numerical methods was achieved provided that the isotherm data be measured over a wide range of adsorbate partial pressures, extending to near the saturation capacity.

Adsorption energy distributions (AEDs) can be calculated from the classical, fundamental integral equation of adsorption using adsorption isotherms and the expectation–maximization method of parameter estimation [105]. The adsorption isotherms are calculated from non-linear elution profiles obtained from GC data using the characteristic points method of finite concentration chromatography. Porous layer open tubular capillary columns are used to support the adsorbent. The performances of these columns are compared to those of packed columns in terms of their ability to supply accurate isotherm data and AEDs. The effect of the finite column efficiency and the limited loading factor on the accuracy of the estimated energy distributions is presented. This accuracy decreases with decreasing efficiency, and approximately 5000 theoretical plates are needed when the loading factor, L_f, equals 0.56 for sampling of a unimodal Gaussian distribution. Increasing L_f further increases the contribution of finite efficiency to the AED, and causes a divergence at the low-energy endpoint if too high. This occurs as the retention time approaches the holdup time. Data are presented for diethyl ether adsorption on a porous silica and its C_{18} bonded derivative. Both the frontal analysis by characteristic points (FACP) and the elution by characteristic points (ECP) methods of GC are presented.

In a paper [106] from 1995, the estimation of adsorption energy distributions from non-linear chromatographic data is considered in detail from both experimental and theoretical viewpoints. The experimental data were obtained on DAVISIL, IMPAQ, and VYDAC silica samples, which were also chemically derivatized. The adsorbates studied included diethyl ether, methanol, ethanol, tetrahydrofuran, pyridine, and heptane. Theoretical models of adsorption included the Langmuir, Jovanovic, Fowler–Guggenheim (both random and patch-wise), and Brunauer–Emmett–Teller local isotherms. The chromatographic data were obtained with the use of high efficiency porous layer open tubular columns. The experimental variables of temperature, and maximum solute partial pressure were studied for their effect on the data and estimation. The validity of the technique was assessed. It was concluded that adsorption energy distributions may only be calculated accurately and without bias for systems in which the majority of the adsorption energy is 10 kJ/mol greater than the heat of vaporization of the solute. For adsorption energies less than this, intermolecular interactions decrease the accuracy and confidence of the results. Other experimental parameters also limit the scope of studies of this kind. The major obstacle in these studies was the difficulty in sampling the entire range of adsorption energies, especially the low energies which correspond to the required measurement of the retention times corresponding to high solute partial pressures.

Finally, a new Jovanovic–Freundlich isotherm model was derived for describing single-component adsorption equilibria on heterogeneous surfaces [107]. The equation was obtained by assuming that the rate of decrease of the fraction of the surface unoccupied by the adsorbate molecules is proportional to a certain power of the partial pressure of the adsorbate. The equation reduces to the Jovanovic equation when the surface becomes homogeneous. At low pressures, the equation reduces to the Freundlich isotherm, but at high pressures a monolayer

coverage is achieved. This model has been applied successfully to the description of the adsorption behavior of a series of chlorinated hydrocarbons on a microporous silica gel, at different temperatures. The monolayer capacity and the heterogeneity parameter exhibit a weak temperature dependence. The third parameter of the model decreases exponentially with increasing temperature. The fit of the experimental data to the new model described was shown to be better than the comparable fits to classical isotherms used for heterogeneous surfaces. The energy distribution function corresponding to the model for Langmuir local adsorption behavior was derived using the Sips procedure and evaluated numerically in a few selected cases.

A numerical method for characterizing heterogeneous solids using GSC data was also published by Heuchel et al. [108]. The numerical regularization method INTEG was employed for determining the distribution function of the adsorption energy from GC measurements. Using Langmuir and Jovanovic local isotherms, the distribution functions were determined for *n*-hexane and 1-hexene on a glass and for cyclohexane and cyclohexene on two silica gels with different pore sizes.

6. Catalytic studies by elution gas chromatography

6.1. Mathematical models

6.1.1. Equilibrium reactors

To our knowledge, the first report on the simultaneous occurrence of a chromatographic separation and a chemical reaction was reported in 1960 by Bassett and Habgood [109]. They investigated the dehydration of cyclopropane to cyclopropene on a molecular sieve and evaluated a first-order rate constant and the heat of adsorption. The plate model was used by Kallen and Heilbronner [110] also in 1960 to investigate a first-order reaction in a chromatographic reactor. Several papers were published during the 1960s covering some theoretical investigations on irreversible first-order reactions by GC. All of them were mainly based on assumptions first explicitly summarized by Langer et al. [111] under the definition of a model of the ideal chromatographic reaction (ICR), as additional idealized reactor model compared to the batch reactor, the continuously stirred tank reactor and the ideal flow column. The correspondence of the rate constants for first-order irreversible reactions from chromatographic and batch reactors was demonstrated by Gil-Av and Herzberg-Minzly [112], Pratt and Langer [113], Langer and Patton [114].

6.1.2. Linear non-equilibrium reactors

The influence of limited adsorption rate constants on the resulting reaction chromatogram was early investigated by Roginzkii and Rozenthal [115] and later by Berman and Yanovskii [116], using analytical solutions of the ideal non-equilibrium model (peak broadening neglected). The influence of diffusion or dispersion effects was first investigated by Roginskii and Rozenthal [117], followed by some other works, like those of Schweich and Villermaux [118,119] using the plate model. The continuous model of chromatography provides a comprehensive insight into all relevant chromatographic processes (dispersion, mass transfer, reaction kinetics). No analytical solution has been found, even in the case of a linear model. However, analytical equations for the statistical moments of the elution peaks can be derived by integral transformation methods, e.g., Laplace transformation. Kocirik [120] was the first to apply this to a chromatographic reactor. More detailed models were used in the investigations of Suzuki and Smith [121,122] and Yamaoka and Nakagawa [123]. There is still the problem that products and reactants cannot generally be completely separated in a chromatographic reactor. Thede et al. [124] evaluated moments for a total chromatogram from product and reactant. However, a quantitative evaluation of statistical moments from experimental data without further assumption (i.e., by integration) requires high precision measurements, which cannot be accomplished with the equipment commercially available for analytical separations.

6.1.3. Reversible reactions

The investigation of reversible first-order reactions became of special interest because of their pharmaceutical background when enantiomerizations are involved. Following theoretical and practical work on the continuous model of chromatography, the

stochastic model and an equation for planar chromatography by Keller and Giddings [125], the possibility to evaluate enantiomerization barriers (free activation enthalpies) was first predicted, then experimentally proved and quantitatively verified by numerical fitting of the plate model to experimental data in the years from 1979 to 1992 by Jung and Schurig [126]. It should be mentioned in this context that the necessity to observe the principle of microscopic reversibility during the evaluation was explicitly pointed out by Bürkle et al. [127]. This leads to considerable possibilities of simplification within evaluations. Recently, an optimized numerical algorithm using parallel computers was used by Hochmuth and König [128]. Stephan et al. [170] and Veciana and Crespo [129] used the fitting of a modified Keller-Giddings equation for the determination of enantiomerization barriers.

6.1.4. Non-linear chromatographic reactors

Investigations of chromatographic reactors with *chromatographic non-linearity* are mainly devoted to preparative chromatographic applications. Papers have been published, e.g. by Schweich and Villermaux [130], which investigate the optimization of product yield considering different types of adsorption isotherms, mainly using numerical techniques. More recently, especially continuous chromatographic reactors were invented and investigated. The available models have been reviewed and characterized by Carr [131].

Linear chromatographic reactors with a *kinetic non-linearity* (i.e., a second-order reaction) were rarely investigated. The early work of Harrison and Koga [132] or Schultz [133] used numerical techniques. As late as in the end of the 1980s, an approximate analytical method for the determination of rate constants was published by Thede et al. [134,135].

6.2. Methods for the determination of rate constants from experimental chromatograms

All methods proposed for the determination of rate constants by elution gas chromatography share, to our knowledge, the following assumptions considering the chromatographic setup: (1) an isothermal column and well-known column temperature; (2) a homogeneous column; (3) uniform flow of the mobile phase; (4) the same reaction order in both phases, with possibly different constants (including zero).

The methods used for the derivation of rate constants from the reaction chromatograms can roughly be divided into three categories, described below in some detail.

6.2.1. Methods related to the peak area (zeroth moment)

Peak area methods can be used for simple first-order and non-first-order reactions, in which the separation of reactant and product is good enough to permit the determination of the conversion with sufficient precision, and in which the reaction is not limited by the mass transfer.

Fig. 11 shows the type of chromatogram, which typically permits the application of the peak area method (one reactant) (cf. also [136,137]). Since the mass transfer must not limit the reaction rate, a simplified balance equation can be written:

$$\frac{\partial c_m}{\partial t} + \frac{V_s}{V_m}\frac{\partial c_s}{\partial t} = -\upsilon\frac{\partial c_m}{\partial x} - \nu_m c_m^n - \frac{V_s}{V_m}\nu k_s c_s^n \tag{102}$$

where c_m, c_s = reactant concentration in the mobile and the stationary phases, respectively; t = time; x = length coordinate along the chromatographic column; υ = linear flow-rate; ν = stoichiometric coefficient; k_m, k_s = reaction rate constant in the mobile and the stationary phases, respectively; n = reaction order; V_m, V_s = volume of the mobile and the stationary phases, respectively.

Comparing Eq. (102) with Eq. (1) of the diffusion section, one sees that a new term was added on the left-hand side describing the rate of concentration change in the solid phase, the longitudinal diffusion term $D_A \partial^2 c_g / \partial x^2$ in the moving phase was omitted, uniformity in the radial direction is assumed, and two new terms pertaining to chemical reactions (in the moving and the stationary phase) have been added on the right-hand side.

Adopting a linear isotherm

$$c_s = K c_m \tag{103}$$

where K is the distribution coefficient between the

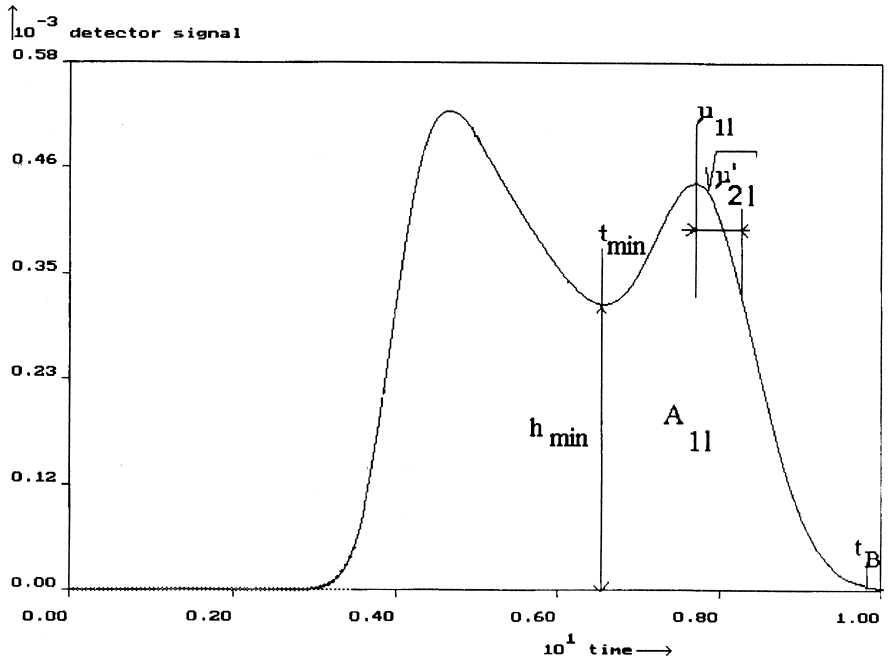

Fig. 11. Type of chromatogram permitting the application of the peak area method (one reactant).

two phases, and defining the partition ratio or retention capacity k as

$$k = \frac{V_s}{V_m} K \tag{104}$$

Eq. (102) can be rearranged to

$$(1+k)\frac{\partial c_m}{\partial t} = -v\frac{\partial c_m}{\partial x} - \nu k_{app} c_m^n \tag{105}$$

where the apparent rate constant k_{app} is given by the relation

$$k_{app} = k_m + kK^{n-1}k_s \tag{106}$$

The evaluation of the rate constants for the mobile phase k_m and the stationary phase k_s is a task which must be solved for any phase or chromatographic system specifically. However, in GC the rate constant in the mobile phase is often zero, since a catalytic reaction takes place with the catalyst dissolved in the stationary phase. Here the true rate constant for the stationary phase can be derived using the net retention time.

Two additional assumptions have been found to be favorable for the derivation of analytical equations: The shape of the reactant peak is given by a Gaussian function Ψ_G at any cross-section of the column, and the statistical moments of this function (retention time, variance) depend linearly on the spatial coordinate:

$$\left\{ \begin{array}{c} c = m\Psi_G \\ \Psi_G = \dfrac{1}{\sqrt{2\pi\mu_2'}} e^{-\frac{(t-\mu_1)^2}{2\mu_2'}} \\ \mu_1 = \dfrac{x}{l}\mu_{1l} \\ \mu_2' = \dfrac{x}{l}\mu_{2l}' \end{array} \right\} \tag{107}$$

where m = zero moment (concentration–time area); μ_1 = first absolute moment; μ_2' = second central moment; l = column length.

These assumptions, the validity of which was discussed elsewhere [138] form a so-called extended ideal chromatographic reactor (EICR). Solutions are found by integrating the mass balance equation over time with an infinite upper limit:

$$\int_0^\infty c\,dt = m, \quad \int_0^\infty \frac{\partial c}{\partial t}dt = 0, \quad \int_0^\infty c^n dt = m^n \int_0^\infty \Psi_G^n dt \tag{108}$$

and solving the system of equations with respect to m. Practically, the following cases are of importance:

(1) First-order reaction ($A_1 \rightarrow P$), with the solution

$$\ln \frac{m_l}{m_o} = -k_a t_o \tag{109}$$

where subscripts o and l mean at column inlet and outlet, respectively, and t_o is the void time.

(2) Second-order reaction of the dimerization type ($2A_1 \rightarrow P$):

$$\frac{m_o}{m_l} = 1 + k_a \frac{2m_o t_o}{\sqrt{\pi \mu'_{2l}}} \tag{110}$$

(3) Second-order reaction of the addition type ($A_1 + A_2 \rightarrow P$): reactions of this type can be carried out by injecting the chromatographically slower reactant first and the chromatographically faster reactant a certain time later. The following solution is found using a respectively modified balance equation and the stoichiometry of the reaction [162]:

$$\ln\left(\frac{m_{1l}}{m_{1o}}\right) - \ln\left(\frac{m_{2l}}{m_{2o}}\right) = k_a t_o (m_{1o} - m_{2o}) \int_0^l \frac{1}{\sqrt{2\pi(\mu'_{21} + \mu'_{22})}} \times \exp\left[-\frac{(\mu_{11} - \mu_{12})^2}{2(\mu'_{21} + \mu'_{22})} \right] d\left(\frac{x}{l}\right) \tag{111}$$

The solution for the stoichiometric case ($m_{1o} = m_{2o}$) can be found from this equation by using Bernoulli-L'Hospital's rule. If the faster reactant overtakes the slower completely within the column, a considerable simplification is possible:

$$\ln\left(\frac{m_{1l}}{m_{1o}}\right) - \ln\left(\frac{m_{2l}}{m_{2o}}\right) = k_a \frac{t_o (m_{1o} - m_{2o})}{|\mu_{11l} - \mu_{12l}|} \tag{112}$$

Zeroth moments at the column inlet (m_{io}, with $i = 1$ or 2) on the right-hand sides of all equations must be considered as concentration–time areas, which can be evaluated from the injected amount of substance and the volume flow-rate (applying James–Martin pressure correction) for the dimerization type, and in the addition type using the volume flow-rate for the pressure at the spatial coordinate, where the peak maxima of both reactants have the same breakthrough time:

$$m_{io} = \frac{n_{io}}{\dot{V}} \tag{113}$$

The ratios of the zeroth moments at the column outlet m_{il} to the zeroth moments at the column inlet m_{io} on the left-hand side of the above equations can be based on the ratio of peak areas to the area of an inert internal standard (*inert standard method*), which is mixed with the respective reactant:

$$\frac{m_{il}}{m_{io}} = \frac{A_{il}}{A_{is}} f_i \quad \text{where} \quad f_i = \frac{A_{is}}{A_{io}} \tag{114}$$

The response factor f_i can be determined from a non-reaction chromatogram of the reaction mixture. For second-order reactions, this can always be managed by decreasing the injection amount. The knowledge of the response factor is obviously not necessary for first-order reactions.

A simplification, known as *product-reactant-method*, is sometimes possible, when stoichiometry and detector response work out in a way that the total area (sum of all peak areas involved) is not changed by the reaction. Then

$$\frac{m_{il}}{m_{io}} = \frac{A_{il}}{A_{\text{total}}} \tag{115}$$

In the case of a simple first-order reaction or of the dimerization type, the co-elution of part of the product under the reactant requires a correction of the reactant pulse area. For first-order reactions, the reactant peak area must be diminished by

$$\Delta A = v_{\text{int}} \int_{t_B}^{t_{\min}} h_{\min} \int_{t_B}^{t} \frac{1}{\sqrt{2\pi\mu'_{2l}}} e^{-\frac{(\tau - \mu_{1l})^2}{2\mu_{2l}'}} d\tau dt \tag{116}$$

where v_{int} = paper speed of integrator; $t_{\min}$ = peak minimum time; $h_{\min}$ = peak minimum height (cf. Fig. 11); t_B = breakthrough time; the use of v_{int} and $h_{\min}$ leads to an area in cm^2. For second-order reactions

$$\Delta A = u_{\text{int}} \int_{t_B}^{t_{\min}} h_{\min} \int_{t_B}^{t} \frac{1}{\sqrt{\pi \mu'_{2l}}} e^{-\frac{(\tau-\mu_{1l})^2}{\mu_{2l}'}} d\tau dt \qquad (117)$$

No area correction is required in the addition type second-order reaction, since complete separation of all reacting partners can be achieved.

Table 2 summarizes the mathematical modelling relating to the peak areas.

Considering the following reasonable limitations for the experimental parameters as: (a) retention times of 10^0 to 10^2 min; (b) theoretical plate numbers of about 10^3; (c) conversion of 10–50% (lower conversions are sensitive to peak area errors, higher conversions to parameter errors); (d) maximum injector concentration not exceeding that of an ideal gas. It can roughly be estimated that the rate constants must range in an interval from 1 to 10^{-4} min^{-1} for first-order and from 10^4 to 10^{-2} dm^3 mol^{-1} min^{-1} in second-order reactions. This applies to the other methods as well.

6.2.2. Methods related to higher statistical moments

These methods are mainly devoted to simple first-order reactions, in which mass transfer limits the chemical reaction. They cannot be used for non-first-order reactions, since no integral transformations of the model equations are possible, and consequently no explicit expressions for the moments can be found. The application of this method with the restrictions mentioned above is only favourable, when a detailed modelling of the chromatographic system is possible and useful. It becomes necessary, if the range of reaction rates and mass transfer rates lie within the same orders of magnitude. It is useful, if the experimental set-up permits high-precision measurements. Therefore, only a general description of the method is given here. For details see Ref. [122].

Table 2
Requirements for the experimental determination of rate constants by the inert standard method

Reaction type	t_o	μ_{1l}	μ'_{2l}	n_o	A_{il}	f_i
A→P	x	x			x	
2A→P	x	x	x	x	x	x
A_1+A_2→P	x	x		x	x	x

The detailed model of the reaction chromatographic process (a set of linear partial differential equations for any reaction partner) is, usually by Laplace transformation, changed to ordinary differential equations which are then solved. From the solution in the Laplace-domain, the zeroth moment, the first absolute moment, the second and third central moments and the fourth semi-invariant can be obtained by the application of the van-der-Laan theorem. If $L(c)$ is the Laplace transformed function of c and p the Laplace variable:

$$m = \lim_{p\to 0} L(c), \quad \mu_1 = \lim_{p\to 0} \frac{d \ln L(c)}{dp},$$

$$\mu'_2 = \lim_{p\to 0} \frac{d^2 \ln L(c)}{dp^2} \qquad (118)$$

$$\mu'_3 = \lim_{p\to 0} \frac{d^3 \ln L(c)}{dp^3}, \quad \mu'_4 - 3\mu'^2_2 = \lim_{p\to 0} \frac{d^4 \ln L(c)}{dp^4} \qquad (119)$$

The cumbersome and tedious manual calculations formerly required can now be completed by symbolic computer programs, like MATHEMATICA or DERIVE. The experimental moments are normally obtained by numerical integration of the concentration for a reaction partner, determined as functions of the flow-rate. Using the theoretical expressions for the moments, the model parameters can be evaluated using non-linear regression and iteration procedures. If the concentration of a single reactant cannot be separately determined, there is still the possibility to use total moments, i.e., to use the sum of all concentrations involved. For the derivation of analytical expression for the total moments, the different detector responses must be known and considered. The simplest total moment of use is the first absolute total moment for an irreversible first-order reaction with same detector responses for reactant and product:

$$\mu_{tl} = \mu_{pl} + \frac{\mu_{Al} - \mu_{pl}}{k_a t_o} (1 - e^{-k_a t_o}) \qquad (120)$$

where μ_{tl} = total moment of the chromatogram; μ_{pl} = first absolute moment of the pure product (non-

reaction conditions); μ_{A1} = first absolute moment of the reactant (non-reaction conditions). Even in this case, non-linear regression is required, and the accuracy of the experimental moment must be better than 0.01 min.

6.2.3. Fitting procedures

These procedures using numerical solutions of the model partial differential equations (PDEs] can be used in principle without any limitation, but the evaluations are still cumbersome, even with large computers. However, their importance will probably increase in the near future. Anyhow, fitting procedures are necessary to evaluate rate constants from chromatograms with more than one reaction involved. Now, there are some approximate chromatogram equations available for complex first-order reactions, which are useful for fast fitting procedures.

Numerical algorithms especially designed for the solution of chromatography models were compared and discussed, i.e., by Czock and Guiochon [139]. These can be in principle extended to reactor applications but only the aforementioned applications by Jung and Schurig [126] or Hochmuth and König [128] are known as examples of a direct determination of rate constants by fitting the numerical solution of the PDEs to experimental results. Recently, it was shown that it is possible to find approximate analytical solutions for the product pulses of simple and complex irreversible first-order reactions via empirical peak shape equations. These were found using the following algorithm: a reactant pulse produces a differential product pulse at any spatial coordinate in the column. The differential product pulse gets its initial retention time and variance from the reactant pulse, but then moves with the velocity of the product and the peak broadening of the product. Any of the product differential pulses can produce its own product pulses, which are of a higher differential order. A concentration element of the respective intermediate or product is given by the differential peak area of a certain differential pulse and its shape, which is defined by a linear combination of first and second moments with respect to the spatial coordinate. The breakthrough concentration of a species at a certain time is given by the sum of all the concentration elements, which at this very time go through the end of the column, i.e., by a suitable integration. Analytical results can be found, if a Gaussian is applied as the peak shape function, and the dependence of the variance on the spatial coordinate is replaced by a medium dependence on time. For details cf. Ref. [167]. Results are available for simple first-order and second-order reactions, first-order consecutive and parallel reactions, and even for first-order reversible reactions, which are treated as six-step consecutive reactions. All experimental testing was done with HPLC, but the equations can be used for gas chromatography as well.

Because of the rather large number of fitting parameters (at least rate constant, retention time and variance for any reaction partner) causing many side minima, the initial values for the parameters must be either obtained from the chromatogram or a grid of initial values must be tried on the chromatogram, choosing optimal initial values out of them.

6.3. Results and conclusions

There are several factors complicating the determination of the rate constants by elution gas chromatography, many of them related to column characteristics, i.e., determination of the phase ratio, interaction with column walls and support, existence of different adsorption sites, or adsorption at a liquid surface, which must be considered individually for the system applied. *Pressure drop* (increasing flow-rate along the spatial coordinate), however, is a complication, which is common to all elution gas chromatographic systems. Fortunately, the determination of apparent rate constants for first-order reactions is not involved, as long as peak area methods and fitting methods based on approximate analytical equations are applied. However, to take full advantage from the high precision method of statistical moments, the pressure drop must be considered in the model calculation [169]. In second-order reactions, the pressure drop acts at least as a dilution for the reactants. Though corrections are possible, pressure ratios of column inlet to column outlet of 1.5–1.7 should preferably not be exceeded. Table 3 lists some reaction examples useful for catalytic studies, and a few comments on the results obtained. The list is not considered comprehensive,

Table 3
Examples of experimental work useful for catalytic studies by elution gas chromatography

Reaction	System	Results	Ref.
Cyclohexene-propylene isomerization	Linde 13X ion exchanger	Rate constant, first-order, adsorption heat, activation energy	[109]
Dehydrogenation of butene to butadiene	Iron oxide catalyst	Improved conversion batch reactor	[164]
Diels-Alders addition in chloromaleic acid	Chloromaleic acid	Rate constant, first-order, activation energy	[165]
Dehydrogenation of cyclohexane to benzene	Heterogeneous Pt catalyst	Comparison of conversion flow tube	[115]
ortho-para-Hydrogen conversion	Molecular sieve	Rate constant, first-order	[140]
Dehydrogenation of cyclohexane to benzene	Several transition metal carbides and silicides	Rate constant, first-order, activation energy	[141]
Diels-Alders reactions with maleic anhydride	Maleic anhydride dissolved in tricresyl-phosphate	Rate constant, first-order, activation energy	[142]
Dehydrogenation of cyclohexane to benzene	Heterogeneous Pt catalyst	Rate constant, first-order	[143]
Esterification of acetic anhydride	Several high-boiling point alcohols	Rate constant, first-order	[144]
Thermal decomposition of pinene	Tricrecylphosphate	Rate constant, first-order	[145]
Dissociation of dicyclo-pentadiene	Apiezon L and similar liquid stationary GC phases	Rate constant, first-order	[113]
IBr-equilibrium	Kel-F	Rate constant, second-order, numerically from plate theory	[132,146]
Cracking of cumene	Heterogeneous oxide catalyst	Possible reversible poisoning of catalyst	[147]
Decomposition of ditertiary butylperoxide	Hexatricontane	Rate constant, first-order, from product chromatogram	[148]
Maleic anhydride and polyisobutylene	Polyisobutylene	Rate constant, first-order	[149]
Esterification of xylenole with acetic anhydride	Squalane	Rate constant, second-order, numerical evaluation	[133]
Substitution of cyclooctene from rhodium (I)-complex	Rhodium salt dissolved in higher alkanes	Equilibrium constants	[150]
Ammonia synthesis	Fe oxide catalyst on a molecular sieve	Conversion as a function of process parameters	[151]
Dissociation of dimer-methylcyclopentadiene	Liquid GC phases	Rate constant, first-order	[152]
p-Toluidine and diphenyl sebacate	Diphenyl sebacate and Apiezon L	Rate constant, first-order	[153]
Dicyclopentadiene dissociation	Polyphenyl ethers, multi-detector and multicolumn reactor	Simultaneous determination of first-order rate constant in both phases by non-linear regression analysis	[154]
Dehydrogenation of ethane	Zeolites covered with cadmium	Conversion, heat of adsorption	[155]
Dehydrogenation of cyclohexane	Heterogeneous Pt catalyst	Conversion as a function of process parameters	[156]
Hydrogenation of cyclohexene	Wilkinson catalyst dissolved in stationary phase	Rate constant, first-order	[157]
Hydrogenation of mesitylene	Pt catalyst in moving bed counter current reactor	Conversion as a function of process parameters	[158]
Hydrogenation of CO	Ni and Ru catalysts	Rate constant, first-order	[159]
Decomposition of organic peroxides	Amphoteric and acidic metal oxides, analytical post-separation	Rate constant, first-order	[160]
Aldol condensation of propionaldehyde	KOH, dissolved in diglycerol	Rate constant, second-order, activation energy	[134]
Dicyclopentadiene dissociation	Liquid crystals	Rate constant, first-order, characterization of stationary phase	[161]
Acylation of aniline	Apiezon L	Rate constant, second-order, activation energy	[162]
Hydrogenation of trimethylbenzene	Polystyrene (Chromosorb 106) mixed with 10% Pt/Al_2O_3	Conversion as a function of process parameters	[163]
Dicyclopentadiene dissociation	Various	Influence of polarity of the stationary phase on rate constant	[168]
Enantiomerization of homofuran, starting from racemate	Polysiloxane anchored Ni(II)–chirasil–metal (complexation GC)	Rate constant, enantiomerization barrier, rev. first-order, fitting of plate model	[166]
Enantiomerization of planar–chiral cyclophanes, starting from racemates	Selectively modified cyclodextrines in polysiloxane solution	Rate constant, enantiomerization barrier, rev. first-order, fitting of plate model	[128]

but references for most cases of practical importance can be found and consulted for details.

7. Catalytic studies by the stopped-flow technique

Most complications in determining rate constants by elution chromatography, as outlined in Section 6.3, are due to the fact that the system being studied is a dynamic continuous flow system with the carrier gas playing a central role. Can't one remove all these difficulties connected with the carrier gas-flow by simply stopping it? No statistical moments, no fitting procedures, no pressure drop corrections, no peak-broadening phenomena, etc., will then have any

physicochemical meaning. The system will be simply switched into a static one. But what about gas chromatography and its role as a separation process of reactants and/or products? This can be achieved by restoring the carrier gas-flow after a short time interval stop and letting it 'separate' what the stopped-flow 'did' as regards catalytic process.

As mentioned in Section 2.2, the stopped-flow technique was introduced in 1967 by Phillips et al. [171] for measuring rate constants of simple surface-catalysed reactions. It requires a very simple experimental set-up, i.e., a slightly modified gas chromatograph, and leads to the determination of, not apparent, but *true* rate constants.

The experimental arrangement is not exactly like that of Fig. 4 (used for diffusion measurements) but that shown in Fig. 12 [172]. A typical reaction chromatogram is given in Fig. 13 [172].

Conder and Young [4] reviewed the stopped-flow technique in 1979, and Powell et al. [159] described various characteristics of the method in conjunction with their investigations of its application to the methanation studies over alumina-supported catalysts. Katsanos in his book published in 1988 [7] devoted a whole chapter to the stopped-flow technique, describing its principle, the various experimental set-ups and the mathematical modelling for its use. It comprises a general theoretical analysis [173], non-opposing reactions on one kind of active sites and no intermediate [174–176], non-opposing reactions on two and three kinds of active sites [177–179], and catalytic conversions [180,181].

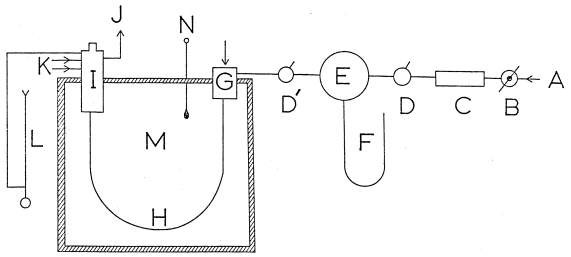

Fig. 12. Arrangement for kinetic studies by the stopped-flow technique. A, carrier gas inlet for the catalytic column; B, control valve; C, gas-drying tube; D, D′, shut-off valves for closing and opening the carrier gas through the column; E, 500-cm^3 volume reservoir to prevent pressure variations during closing and opening the gas flow; F, open manometer to detect pressure variations and measure the pressure drop along the catalytic column; G, injector to the column heated at oven temperature; H, catalytic column; I, flame ionization detector; K, hydrogen and air to the detector; J, signal to amplifier and recorder; L, bubble flowmeter; M, gas chromatograph oven; N, thermometer [172].

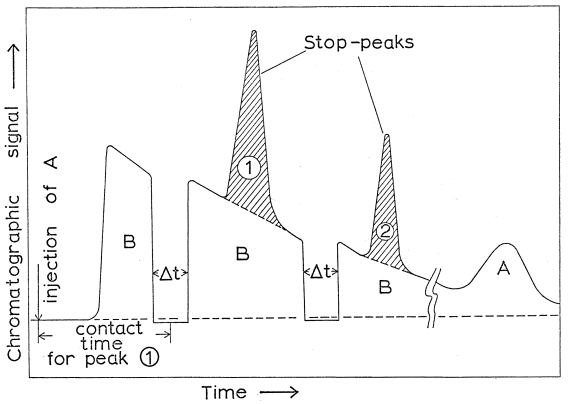

Fig. 13. Gas chromatographic trace showing the stopping of the carrier gas through the column for time Δt. The extra peaks 1 and 2 appear after restoring the carrier gas flow [172].

As pointed out by Powell and Langer [182] in studying low-temperature methanation and Fischer–Tropsch activity over supported catalysts, the stopped-flow gas chromatographic reactor is a sensitive technique to measure very low rates of reactions, not requiring sampling for analysis in a separate system.

8. Simultaneous diffusion, adsorption and catalytic measurements

As mentioned at the end of Section 1, there is a method permitting the determination of diffusion parameters, adsorption/desorption rate constants and isotherms, and catalytic rate constants, all these simultaneously in a single gas chromatographic experiment. The method is based on the RF-GC technique, already described in Section 2.3 and Section 2.4 for the determination of diffusion coefficients in gases and obstruction factors, in Section 3.3 for measuring diffusion coefficients of gases in liquids, and in Section 5.3 for simple determination of experimental adsorption isotherms. In the latter case a wide range of concentrations is covered, a specification of an a priori isotherm equation is not required, and the rate constant of a surface reaction of the adsorbed solute is measured simultaneously with the desorption rate constant of the solute [83].

The experimental arrangement resembles that depicted in Fig. 5 for diffusion coefficient measurements, differing only in the diffusion denuder tube covered with a thin layer of the solid adsorbent, catalyst, etc., on its internal wall (cf. Fig. 14A). In addition to the original publication [83], an extended summary of the mathematical modelling and calculations are given in a more recent review [84].

Since 1995 two more advances have been achieved: (a) the adsorption and catalytic measurements were rendered independent of the diffusion coefficient of reactant(s), which until then was determined independently or found in the literature or calculated theoretically (cf. Section 2), under different conditions, and used with the adsorption and catalytic calculations (cf. Ref. [83]); (b) the experimental set-up does not comprise a denuder tube as in Fig. 14, but an ordinary catalytic bed, the solid adsorbent or catalyst filling a relatively small length L_2 of the diffusion column L_1+L_2 in its total internal diameter with an external porosity ϵ. This arrangement is shown in Fig. 15 and it was first used by us for catalytic studies in 1995 [183], based on a linear isotherm. This type resembles a plug flow reactor, but without a gas flowing through it. It is a gaseous diffusion current of the reactant(s) and product(s) that causes the movement of these substances through the solid bed along the coordinate y, and then along coordinate z to the junction $x=l'$ of the sampling column. Thus, two diffusion coefficients are involved in these movements: one in section $L_1(D_1)$ and another in section $L_2(D_2)$ influenced by the bed obstruction factor γ. All these are taken care of implicitly in the mathematical analysis, without using the actual values of the diffusion coefficients D_1 and D_2. On the contrary, the latter can be calculated from the diffusion parameters α_1 and α_2 (cf. Eq. (132) in Section 8.2), which are printed by the PC program used, along with the other physicochemical parameters.

8.1. Experimental procedure and calculations

Each kinetic run is carried out as described in Section 2.3 and consists in reversing the direction of the carrier gas flow through the sampling column (depicted in Fig. 15) for 10–60 s repeatedly. Then, the height H (say in cm) from the ending baseline (or the area under the curve) of each extra *sample peak*, created by each flow-reversal, is recorded, together with the respective time t passed from the reactant injection until the flow-reversal. So, one is left with a long series of pair values H, t (say 30–80) and no other experimental result or correction is needed for the calculation of the kinetic data k_1, k_{-1} and k_2 of the reaction, except for the response factor M of the detector (1 for FID and thermal conductivity detection, 1–2 for flame photometric detection, etc.), the lengths L_1 and L_2 of the diffusion column, the

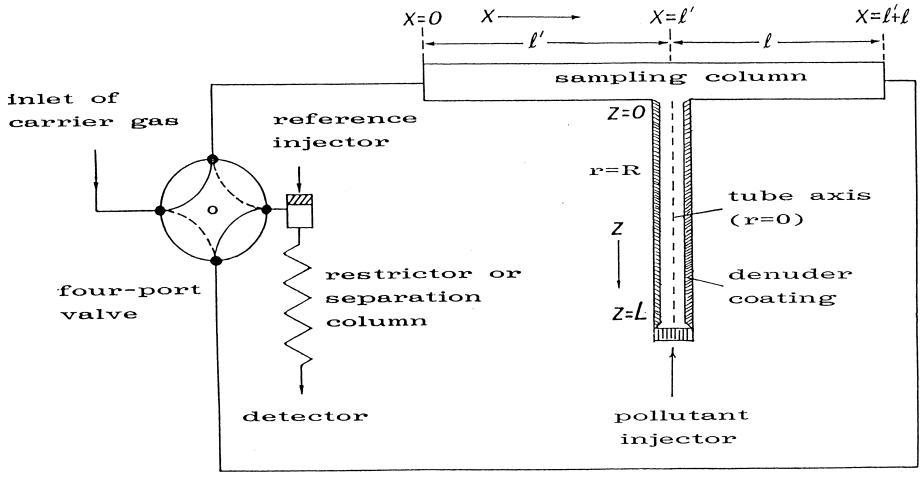

Fig. 14. Schematic representation of gas connections and columns for carrying out simultaneous diffusion, adsorption and catalytic measurements with a diffusion denuder tube [83].

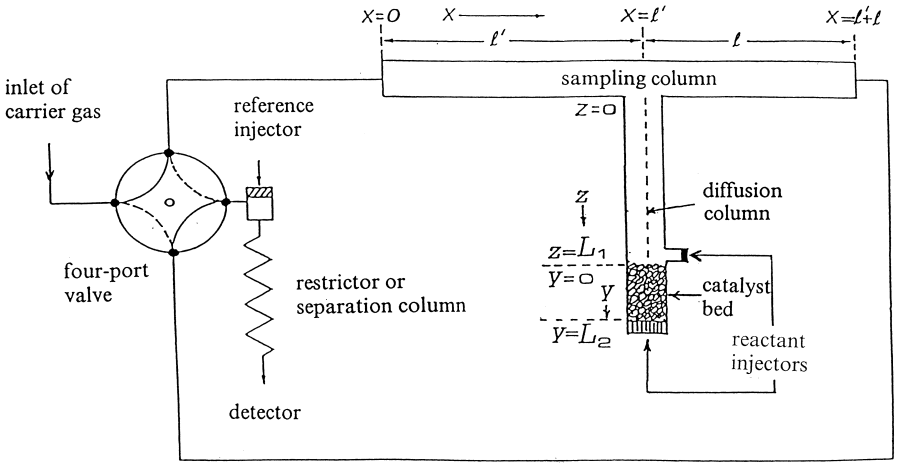

Fig. 15. Schematic representation of columns and gas connections in catalytic studies, with simultaneous measurement of diffusion coefficients and adsorption isotherms, employing an ordinary catalytic bed [185].

gaseous volumes V_{G1} and V_{G2} of the empty sections L_1 and L_2, respectively, and the external porosity ϵ of the solid bed. If the deposition velocity V_d of the reactant on the solid surface and its reaction probability γ with it are wanted, one must know the cross-sectional area a_y of the void space in region y, the amount of solid per unit length of column a_s, the specific surface area of solid SSA, the molar mass of the solute M_B, and the temperature T of the reaction cell (usually thermostated inside the chromatographic oven). Finally, if one wants also the experimental adsorption isotherm of reactant to be printed point by point, the corrected volumetric flow-rate of the carrier gas $\dot{V}$ and the amount of analyte injected n_A are required. If not, the real experimental isotherm will not be printed, but it will be taken into account in the calculations automatically.

By entering the pairs of values H, t in the DATA lines 3000–3040 of the PC program in GW-BASIC listed in Appendix A, together with the other quantities mentioned above in the INPUT lines 160–330, this program calculates first the pre-exponential factors A_1, A_2, A_3 and A_4, together with the exponential coefficients of time B_1, B_2, B_3 and B_4 of the function

$$H_4^{1/M} = gc(l',t) = A_1 \exp(B_1 t) + A_2 \exp(B_2 t) + A_3 \exp(B_3 t) + A_4 \exp(B_4 t) \quad (121)$$

and then the respective values of A_5, A_6 and A_7, and B_5, B_6 and B_7 of the function

$$H_3^{1/M} = gc(l',t) = A_5 \exp(B_5 t) + A_6 \exp(B_6 t) + A_7 \exp(B_7 t) \quad (122)$$

where g is a calibration factor of the detector used and $c(l',t)$ the concentration of the solute at the junction $x=l'$ at time t. Both above equations give the height H of the sample peaks as a sum of exponential functions of time t, using two different approximations, i.e., a four-exponential and a three-exponential function H_4 and H_3, respectively.

It is the theoretical analysis described in Section 8.2 which leads to the conclusion that the function $H=f(t)$ has the form of Eq. (121) or Eq. (122), with all B values being negative and A values being either positive or negative. The PC program in Appendix A, mentioned above, calculates the values of A and B values by non-linear regression analysis, based on a Fortran IV computer program of Sedman and Wagner [184], dealing with polyexponential parameter estimates. As one can see from Appendix A (cf. lines 20 and 30), the program is not a single seven-exponential function for extracting $B_1, B_2, \ldots, B_7$ from the experimental H, t values, but two functions, one with four exponentials and the other with three exponentials according to Eq. (121) and Eq. (122). The exponential stripping method is guided by the overall

goodness of fit expressed by the square of correlation coefficient r^2. This universally accepted criterion is calculated according to Eq. (5) of Ref. [184]. The maximum values of r^2 for the four- and three-exponential functions finally selected are printed in the lines 1290 and 2050, respectively. In most cases studied by ourselves, they were in the range 0.991–0.999, showing a remarkable goodness of fit for a non-linear regression analysis. The *t*-test of significance for the smallest r^2 found shows that it is highly significant, with a probability to be exceeded smaller than 0.05%. The program also prints, together with the *B* values, their standard errors (cf. lines 1180, 1210, 1240, 1270, 1970, 2000 and 2030 for B_1, B_2, B_3, B_4, B_5, B_6 and B_7, respectively). The errors found in all runs carried out by ourselves are reasonable for physicochemical measurements.

8.2. Mathematical model

The main lines of the necessary theoretical analysis based on the arrangement of Fig. 15 are given below, by assuming a non-linear adsorption isotherm, defined as

$$c_s^* = \frac{a_y}{a_s} k_1 \int_0^t c_y(\tau)\mathrm{d}\tau \quad \text{or}$$

$$c_s^* = \frac{n_s}{a_s}\delta(y - L_2) + \frac{a_y}{a_s} k_1 \int_0^t c_y(\tau)\mathrm{d}\tau \qquad (123)$$

Either the first or the second equation is used, depending on whether the reactant A is injected as an instantaneous pulse (delta function, δ) at $z = L_1$ (first equation) or at $y = L_2$ (second equation).

The symbols above are: c_s^* = equilibrium adsorbed concentration of analyte at time *t*, mol/g; n_s = initially adsorbed equilibrium amount of analyte, mol; a_s = amount of solid adsorbent or catalyst per unit length of column bed, g/cm; y = length coordinate along section L_2, cm; c_y = gaseous concentration of the analyte in region *y*, mol/cm^3; a_y = cross-sectional area of the void space in region *y*, cm^2; $\delta(y - L_2)$ = Dirac's delta function describing the initial condition of the bed, when the analyte is introduced as an instantaneous pulse at the point $y = L_2$, cm^{-1}; k_1 = dynamic adsorption rate constant describing the local experimental isotherm of the analyte on the solid surface, varying with time, s^{-1}; τ = dummy variable for time.

The mass balance equation in the filled region *y* of the diffusion column is

$$\frac{\partial c_y}{\partial t} = D_2 \frac{\partial^2 c_y}{\partial y^2} - k_{-1}\frac{a_s}{a_y}(c_s^* - c_s) \qquad (124)$$

where D_2 = diffusion coefficient of the analyte in section L_2, cm^2/s; k_{-1} = rate constant for desorption from the bulk solid, s^{-1}; c_s = concentration of analyte adsorbed on the solid at time *t*, mol/g.

The rate of change of the adsorbed concentration is described by the relation

$$\frac{\partial c_s}{\partial t} = k_{-1}(c_s^* - c_s) - k_2 c_s \qquad (125)$$

where k_2 (s^{-1}) is the rate constant of a possible first-order or pseudo-first-order surface reaction of the adsorbed reactant A.

The initial conditions are

$$c_y(0,y) = \frac{n_A}{a_y}\delta(y - L_2) \quad \text{and} \quad c_s(0,y) = 0 \qquad (126)$$

where n_A is the amount (mol) of analyte introduced as a pulse at $y = L_2$.

In gaseous region *z* the diffusion equation for the analyte A is

$$\frac{\partial c_z}{\partial t} = D_1 \frac{\partial^2 c_z}{\partial z^2} \qquad (127)$$

where z = length coordinate along section L_1, cm; c_z = gaseous concentration of analyte in *z*, mol/cm^3; D_1 = diffusion coefficient of analyte in L_1, cm^2/s.

The system of partial differential Eq. (124), Eq. (125) and Eq. (127) is solved by using double Laplace transforms of all terms with respect to time and length coordinates, under the initial conditions Eq. (126) and $c_z(0,z) = 0$, the isotherm Eq. (123), and subject to the appropriate boundary conditions at the junctions L_2/L_1 and $x = l'$ (cf. Fig. 15). The result, by means of certain approximations [84], leads to Eq. (121). The physical meaning of the exponential coefficients of time B_1, B_2, B_3 and B_4 are as follows:

$$\alpha_2(1 + V_1) + k_{-1} + k_2 = -(B_1 + B_2 + B_3 + B_4) = X \qquad (128)$$

$$\alpha_2(1+V_1)(k_{-1}+k_2)+\alpha_1\alpha_2+k_1k_{-1}=B_1B_2+B_1B_3+B_1B_4+B_2B_3+B_2B_4+B_3B_4=Y \quad (129)$$

$$\alpha_1\alpha_2(k_{-1}+k_2)+\alpha_2V_1k_1k_{-1}+k_1k_{-1}k_2=-(B_1B_2B_3+B_1B_2B_4+B_1B_3B_4+B_2B_3B_4)=Z \quad (130)$$

$$\alpha_2V_1k_1k_{-1}k_2=B_1B_2B_3B_4=W \quad (131)$$

where

$$\alpha_1=2D_1/L_1^2 \quad \text{and} \quad \alpha_2=2D_2/L_2^2 \quad (132)$$

$$V_1=\frac{2V_{G2}(\text{empty})\epsilon}{V_{G1}}+\frac{L_2^2}{L_1^2} \quad (133)$$

In order that diffusion coefficients in Eq. (132) are not obtained from other sources, one can use a steady-state approximation for c_s in Eq. (125), $dc_s/dt=0$, leading to

$$k_{-1}(c_s^*-c_s)-k_2c_s=0 \quad (134)$$

Using this in place of Eq. (125), there results Eq. (122) instead of Eq. (121), B_5, B_6 and B_7 having the content:

$$\alpha_2(1+V_1)=-(B_5+B_6+B_7)=X_1 \quad (135)$$

$$\alpha_1\alpha_2+\frac{k_1k_{-1}k_2}{k_{-1}+k_2}=B_5B_6+B_5B_7+B_6B_7=Y_1 \quad (136)$$

$$\frac{\alpha_2V_1k_1k_{-1}k_2}{k_{-1}+k_2}=-(B_5B_6B_7)=Z_1 \quad (137)$$

From the seven auxiliary parameters X, Y, Z, W, and X_1, Y_1, Z_1, defined by Eqs. (128)–(131) and Eqs. (135)–(137), respectively, one can calculate the three main physicochemical parameters k_1, k_{-1} and k_2, without the use of D_1 and D_2. The PC program in GW-BASIC of Appendix A has been written for this purpose also, giving directly k_1, k_{-1} and k_2.

From these parameters, the deposition velocity V_d of the gaseous analyte on the surface of the catalyst, and the reaction probability γ with that are calculated by the simple mathematical formulae

$$V_d=\frac{k_1V_{G2}(\text{empty})\epsilon}{A_s}\cdot\frac{k_2}{k_{-1}+k_2} \quad (138)$$

$$\frac{1}{\gamma}=\left(\frac{R_gT}{2\pi M_B}\right)^{1/2}\cdot\frac{1}{V_d}+\frac{1}{2} \quad (139)$$

where A_s is the total surface area of the solid (cm^2), R_g the ideal gas constant, T the absolute temperature and M_B the molar mass of the gaseous analyte. The values of these two additional parameters, V_d and γ, are also displayed by running the PC program of Appendix A, provided T, a_s, SSA and M_B are entered in the INPUT lines 200, 270, 280 and 290, respectively.

It is clear from the definition of V_d by Eq. (138) and the relation of γ with it (Eq. (139)), that both parameters are independent of molecular diffusion, being related only to the local adsorption isotherm (k_1), the desorption rate constant (k_{-1}) and the surface reaction rate constant (k_2).

The explicit calculation of the isotherms can be carried out as described elsewhere [83]. However, the following equations are improved, as they are based on Eq. (121) rather than Eq. (122), as was done originally [83]:

$$\frac{\partial c_s^*}{\partial c_g}=k_1\frac{a_y\sum_{i=1}^{4}A_i\exp(B_it)}{a_s\sum_{i=1}^{4}A_iB_i\exp(B_it)} \quad (140)$$

$$c_s^*=\frac{k_1a_y}{ga_s}\sum_{i=1}^{4}A_i[\exp(B_it)-1]/B_i \quad (141)$$

$$c_g=\frac{1}{g}\sum_{i=1}^{4}A_i\exp(B_it) \quad (142)$$

where c_g is the gaseous concentration of the solute (mol/cm^3), A_i and B_i are the pre-exponential factors and the exponential coefficients of Eq. (121), and g in $cm/(mol\ cm^{-3})$ is the proportionality constant between peak height H (cm) and gaseous concentration of the analyte c_g ($mol\ cm^{-3}$). One can consider t in the above equations as a dummy independent variable and calculate, for chosen arbitrary values of t, both the differential isotherm $\partial c_s^*/\partial c_g$ and c_s^* together with the corresponding values of c_g. Plotting $\partial c_s^*/\partial c_g$ or c_s^* against c_g for each chosen t, independent experimental isotherms are obtained.

By entering an initial time T_1 and a final time T_2 in the 320 and 330 INPUT lines of the PC program given in Appendix A, this calculates and prints g, $\partial c_s^*/\partial c_g$, c_s^* and c_g, together with the other parameters mentioned before.

A similar model, but with a simultaneous interaction in the gas phase between the solute A and another gaseous solute B leads to the calculation of an apparent rate constant of a gaseous reaction between A and B, in addition to the physicochemical parameters k_1, k_{-1}, k_2, V_d and γ, mentioned above. This model has already been published [185], together with another work [186] in which the methodology was applied to the reactions between volatile hydrocarbons and inorganic pigments, under the influence of gaseous nitrogen dioxide.

Acknowledgements

The last section of this review (Section 8) has been based on the work carried out within the frame of Contract EV 5V-CT94-0537 of the European Commission, DG-XII. Two of the authors (N.A.K. and F.R.K.) warmly acknowledge this financial support. The help of Mrs. Margaret Barkoula and Miss Anna Malliori in the typescript preparation is also acknowledged.

Appendix A

```
10 REM Non-Linear Regression Analysis of Functions:
20 REM H^(1/M)=A1*EXP(B1*T)+S*A2*EXP(B2*T)+P*A3*EXP(B3*T)+X*A4*EXP(B4*T)
30 REM H^(1/M)=A5*EXP(B5*T)+S*A6*EXP(B6*T)+P*A7*EXP(B7)
40 REM Calculation of kinetic parameters and isotherms with the experimental
       setup of Chromatographia 41(1995)227,with injection of one substance, at
       y=0 or y=L2.
50 REM     N2     = Minimum number of points of first exponential function
60 REM     MAX    = Square of maximum correlation coefficient
70 REM     OPT    = Final optional choice of variables when OPT=1
80 REM     J      = Number of points of first exponential function
90 REM     G      = Number of points of second exponential function
100 REM     F      = Number of points of third exponential function
110 REM    K,L    = First and last point of linear regression in subroutine
120 REM    SA,SB  = Standard errors of A and B in each linear regression
130 REM    Y(I)   = Ordinate for each linear regression in the subroutine
140 REM    U(I)   = Variable remaining by  removal of the previous one, two or
                    three exponential functions
150 REM    D(I)   = Function for calculating the squared correlation coefficient
160 INPUT "Total number of pairs H,T=";N
170 DIM H(N),T(N),Y(N),U(N),D(N)
180 INPUT "Response factor=";M
190 INPUT "Factor to divide H(I)=";H1
200 INPUT "Temperature in K=";T0
210 INPUT "Lenth L1(cm) of Section z=";L1
220 INPUT "Length L2(cm) of Section y=";L2
230 INPUT "Gaseous Volume VG1(cm^3) of Empty Section L1=";VG1
240 INPUT "Gaseous Volume VG2(cm^3) of Empty Section L2=";VG2
250 INPUT "External Porosity E of the Solid bed=";E
260 INPUT "Cross Sectional Area AY(cm^2) of Void Space in Region y=";AY
270 INPUT "Amount of Adsorbent per Unit Length of Bed AS(g/cm)=";AS
280 INPUT "Specific Surface Area SSA(cm^2/g) of Solid=";SSA
290 INPUT "Molar Mass MB(kg/mol) of the Analyte B=";MB
300 INPUT "Flow-rate of Carrier Gas V'(cm^3/s)=";V0
310 INPUT "Amount of Reactant injected NB(mol)=";NB
320 INPUT "Initial Time T1(min) for the Calculation of the Isotherm=";T1
330 INPUT "Final Time  T2(min) for the Calculation of the Isotherm=";T2
340   FOR I=1 TO N
350    READ H(I),T(I)
360    H(I)=H(I)/H1
370   NEXT I
380 N2=INT(N/7+.5)
390 MAX=0:OPT=0
400 REM Calculation of A1 and B1 with H,T pairs ranging from N2 to N-2*N2-3
410 FOR J=N2 TO N-2*N2-3
420    K=N-J+1
430    L=N
440    FOR I=K TO L
450       Y(I)=(1/M)*LOG(H(I))
460    NEXT I
470    GOSUB 4000       :REM Subroutine for linear regression analysis
480    A1=EXP(A)
490    B1=B
500    SA1=SA
510    SB1=SB
520    IF OPT=1 THEN  560
530 REM Calculation of A2 and B2 with H,T pairs ranging from N2 to N-J-N2-3
       ,and both prefixes -1 or +1
540    FOR S=-1 TO +1 STEP 2
550       FOR G=N2 TO N-J-N2-3
560          K=N-J-G+1
570           L=N-J
580          FOR I=K TO L
590             U(I)=S*H(I)^(1/M)-S*A1*EXP(B1*T(I))
600             Y(I)=LOG(ABS(U(I)))
610          NEXT I
```

```
620          GOSUB 4000    :REM Subroutine for linear regression analysis
630          A2=EXP(A)
640          B2=B
650          SA2=SA
660          SB2=SB
670          IF OPT=1 THEN 710
680 REM Calculation of A3 and B3 with H,T pairs ranging from N2 to N-J-G-3
     and both prefixes -1 or +1
690          FOR P=-1 TO +1 STEP 2
700             FOR F=N2 TO N-J-G-3
710                K=N-J-G-F+1
720                 L=N-J-G
730                FOR I=K TO L
740                   U(I)=P*(H(I)^(1/M)-A1*EXP(B1*T(I))-S*A2*EXP(B2*T(I)))
750                   Y(I)=LOG(ABS(U(I)))
760                NEXT I
770                GOSUB 4000    :REM Subroutine for linear regression analysis
780                A3=EXP(A)
790                B3=B
800                SA3=SA
810                SB3=SB
820                IF OPT=1 THEN 850
830 REM Calculation of A4 and B4 with H,T pairs ranging from 1 to N-J-G-F,and
     both prefixes -1 or +1
840                FOR X=-1 TO +1 STEP 2
850                   K=1
860                   L=N-J-G-F
870                   FOR I=K TO L
880                      U(I)=X*(H(I)^(1/M)-A1*EXP(B1*T(I))-S*A2*EXP(B2*T(I))-P*
                              A3*EXP(B3*T(I)))
890                      Y(I)=LOG(ABS(U(I)))
900                   NEXT I
910                   GOSUB 4000  :REM Subroutine for linear regression analysis
920                   A4=EXP(A)
930                   B4=B
940                   SA4=SA
950                   SB4=SB
960                   IF OPT=1 THEN 1170
970                   C1=0
980                   C2=0
990                   C3=0
1000                   FOR I=1 TO N
1010                      D(I)=H(I)^(1/M)-A1*EXP(B1*T(I))-S*A2*EXP(B2*T(I))-P*A3
                              *EXP(B3*T(I))-X*A4*EXP(B4*T(I))
1020                      C1=C1+D(I)^2
1030                      C2=C2+H(I)^(2/M)
1040                      C3=C3+H(I)^(1/M)
1050                   NEXT I
1060                   R=1-C1/(C2-C3^2/N)
1070                   IF R>MAX THEN MAX=R:SMAX=S:PMAX=P:XMAX=X:JMAX=J:GMAX=G:
                         FMAX=F
1080 PRINT MAX
1090                NEXT X
1100             NEXT F
1110          NEXT P
1120       NEXT G
1130    NEXT S
1140 NEXT J
1150 S=SMAX:P=PMAX:X=XMAX:J=JMAX:G=GMAX:F=FMAX:OPT=1
1160 GOTO 420
1170 LPRINT "Intercept Ln(A1) and its Standard error =";LOG(A1*H1) "+-"SA1
1180 LPRINT "Slope B1 and its Standard error=";B1 "+-"SB1
1190 LPRINT
1200 LPRINT "Intercept Ln(A2) and its Standard error=";LOG(A2*H1) "+-"SA2
1210 LPRINT "Slope B2 and its Standard error=";B2 "+-"SB2
```

```
1220 LPRINT
1230 LPRINT "Intercept Ln(A3) and its Standard error=";LOG(A3*H1) "+-"SA3
1240 LPRINT "Slope B3 and its Standard error=";B3 "+-"SB3
1250 LPRINT
1260 LPRINT "Intercept Ln(A4) and its Standard error=";LOG(A4*H1) "+-"SA4
1270 LPRINT "Slope B4 and its Standard error=";B4 "+-"SB4
1280 LPRINT
1290 LPRINT "Square of maximum correlation coefficient r^2=";MAX
1300 LPRINT "Optimum values of points for 1st, 2nd , 3rd and 4th exponential
       functions, respectively=";JMAX","GMAX","FMAX"and"N-JMAX-GMAX-FMAX
1310 LPRINT "Values of S,P and X,respectively ="; SMAX","PMAX"and"XMAX
1320 S0=SMAX:P0=PMAX:X0=XMAX
1330 LPRINT
1340 N2=INT(N/6+.5)
1350 MAX=0:OPT=0
1360  REM Calculation of A5 and B5 with H,T pairs ranging from N2 to N-N2-3
1370 FOR J=N2 TO N-N2-3
1380    K=N-J+1
1390    L=N
1400    FOR I=K TO L
1410       Y(I)=(1/M)*LOG(H(I))
1420    NEXT I
1430    GOSUB 4000        : REM Subroutine for linear regression analysis
1440    A5=EXP(A)
1450    B5=B
1460    SA5=SA
1470    SB5=SB
1480    IF OPT=1 THEN  1520
1490  REM Calculation of A6 and B6 with H,T pairs ranging from N2 to N-J-3 and
        both prefixes -1 and +1
1500    FOR S=-1 TO +1  STEP 2
1510       FOR G=N2 TO N-J-3
1520          K=N-J-G+1
1530          L=N-J
1540          FOR I=K TO L
1550             U(I)=S*H(I)^(1/M)-S*A5*EXP(B5*T(I))
1560             Y(I)=LOG(ABS(U(I)))
1570          NEXT I
1580          GOSUB 4000     : REM Subroutine for linear regression analysis
1590          A6=EXP(A)
1600          B6=B
1610          SA6=SA
1620          SB6=SB
1630          IF OPT=1 THEN 1660
1640  REM Calculation of A7 and B7 with H,T pairs ranging from 1 to N-J-G,
        with both prefixes -1 and +1
1650          FOR P=-1 TO +1 STEP 2
1660             K=1
1670             L=N-J-G
1680             FOR I=K TO L
1690                U(I)=P*(H(I)^(1/M)-A5*EXP(B5*T(I))-S*A6*EXP(B6*T(I)))
1700                Y(I)=LOG(ABS(U(I)))
1710             NEXT I
1720             GOSUB 4000    : REM Subroutine for linear regression analysis
1730             A7=EXP(A)
1740             B7=B
1750             SA7=SA
1760             SB7=SB
1770             IF OPT=1 THEN 1960
1780             C1=0
1790             C2=0
1800             C3=0
1810             FOR I=1 TO N
1820                D(I)=H(I)^(1/M)-A5*EXP(B5*T(I))-S*A6*EXP(B6*T(I))
                        -P*A7*EXP(B7*T(I))
```

```
1830                C1=C1+D(I)^2
1840                C2=C2+H(I)^(2/M)
1850                C3=C3+H(I)^(1/M)
1860             NEXT I
1870             R=1-C1/(C2-C3^2/N)
1880             IF R>MAX THEN MAX=R:SMAX=S:PMAX=P:JMAX=J:GMAX=G
1890 PRINT MAX
1900          NEXT P
1910       NEXT G
1920    NEXT S
1930 NEXT J
1940 S=SMAX:P=PMAX:J=JMAX:G=GMAX:OPT=1
1950 GOTO 1380
1960 LPRINT "Intercept Ln(A5) and its Standard error=";LOG(A5*H1) "+-"SA5
1970 LPRINT "Slope B5 and its Standard error=";B5 "+-"SB5
1980 LPRINT
1990 LPRINT "Intercept Ln(A6) and its Standard error=";LOG(A6*H1) "+-"SA6
2000 LPRINT "Slope B6 and its Standard error=";B6 "+-"SB6
2010 LPRINT
2020 LPRINT "Intercept Ln(A7) and its Standard error=";LOG(A7*H1) "+-"SA7
2030 LPRINT "Slope B7 and its Standard error=";B7 "+-"SB7
2040 LPRINT
2050 LPRINT "Square of maximum correlation coefficient r^2=";MAX
2060 LPRINT "Optimum values of points for 1st, 2nd and 3rd exponential
          functions,respectively=";JMAX","GMAX"and"N-JMAX-GMAX
2070 LPRINT "Values of S and P, respectively =";SMAX"and"PMAX
2080 LPRINT
3000 DATA
3010 DATA
3020 DATA
3030 DATA
3040 DATA
3050 X=-(B1+B2+B3+B4)/60
3060 Y=(B1*B2+B1*B3+B1*B4+B2*B3+B2*B4+B3*B4)/60^2
3070 Z=-(B1*B2*B3+B1*B2*B4+B1*B3*B4+B2*B3*B4)/60^3
3080 W=(B1*B2*B3*B4)/60^4
3090 X1=-(B5+B6+B7)/60
3100 Y1=(B5*B6+B5*B7+B6*B7)/60^2
3110 Z1=-(B5*B6*B7)/60^3
3120 V1=2*VG2*E/VG1+(L2^2/L1^2)
3130 SK(1)=X-X1:SK(2)=W/Z1:SK(3)=(SK(1)+SK(2))/2:REM  SK=k_1+k2
3140    FOR I=1 TO 3
3150 AV=X-SK(I)
3160 A2V1=AV*V1/(1+V1)
3170 A20=AV/(1+V1)
3180 K1K3=(Y-AV*SK(I)-Z/SK(I)+W/A2V1/SK(I))/(1-A2V1/SK(I))
3190 K1K3=ABS(K1K3)
3200 K2=W/A2V1/K1K3
3210 K3=SK(I)-K2 :K3=ABS(K3)
3220 K1=K1K3/K3
3230 A11 =(Y-AV*SK(I)-K1K3)/A20
3240 A12=(Z-A2V1*K1K3-K1K3*K2)/SK(I)/A20
3250 VD=K1*VG2*E*K2/(SSA*AS*L2*SK(I))
3260 G10=SQR(1.32321*T0/MB)/VD*100+.5
3270 G2=1/G10
3280  LPRINT "k1 in 1/s=";K1
3290  LPRINT "k_1 in 1/s=";K3
3300  LPRINT "k2 in 1/s=";K2
3310 LPRINT "Deposition Velocity in cm/s=";VD
3320 LPRINT "Reaction Probability =";G2
3330 LPRINT "a2(1+V1) in 1/s=";AV",a2 in 1/s=";A20",a1 in 1/s=";A11",";A12
3340 LPRINT
3350 NEXT I
3360 B1=B1/60:B2=B2/60:B3=B3/60:B4=B4/60
3370 A1=A1*H1:A2=S0*A2*H1:A3=P0*A3*H1:A4=X0*A4*H1
```

```
3380 A=A1/B1+A2/B2+A3/B3+A4/B4
3390 G1=-V0*A/NB
3400 LPRINT "Calibration Factor of Detector g'in cm per mol/cm^3=";G1
3410 LPRINT
3420 LPRINT TAB(1);"Time(min)";TAB(17);"dCS/dCG(cm^3/g)";TAB(35);"CS(mol/g)";TAB
(50);"CG(mol/cm^3)"
3430 T1=T1*60:T2=T2*60
3440 FOR T=T1 TO T2 STEP 300
3450   DCS=(K1*AY*E/AS)*(A1*EXP(B1*T)+A2*EXP(B2*T)+A3*EXP(B3*T)+A4*EXP(B4*T))/(A
1*B1*EXP(B1*T)+A2*B2*EXP(B2*T)+A3*B3*EXP(B3*T)+A4*B4*EXP(B4*T))
3460   CS=-(K1*AY*E/AS/G1)*(A1*EXP(B1*T)/B1+A2*EXP(B2*T)/B2+A3*EXP(B3*T)/B3+A4*E
XP(B4*T)/B4)
3470   CG=(A1*EXP(B1*T)+A2*EXP(B2*T)+A3*EXP(B3*T)+A4*EXP(B4*T))/G1
3480 LPRINT TAB(1);T/60;TAB(15);DCS;TAB(30);CS;TAB(45);CG
3490 NEXT T
3500 END
4000  REM Linear regression of Y(I) = A + B T(I)
4010 S1=0
4020 S2=0
4030 S3=0
4040 S4=0
4050 S5=0
4060    FOR I=K TO L
4070    S1=S1+T(I)
4080    S2=S2+T(I)^2
4090    S3=S3+Y(I)
4100    S4=S4+Y(I)^2
4110    S5=S5+T(I)*Y(I)
4120 NEXT I
4130 Z=L-K+1  :REM Number of points for the linear regression analysis
4140 M1=S5-S1*S3/Z
4150 M2=S2-S1^2/Z
4160 M3=S4-S3^2/Z
4170 A=(S3-S1*M1/M2)/Z
4180 B=M1/M2
4190 SYT=SQR(ABS(S4-A*S3-B*S5)/(Z-2))
4200 SA=SYT*SQR(S2/Z/M2)
4210 SB=SYT/SQR(M2)
4220 RETURN
```

References

[1] O.A. Hougen, K.M. Watson, Chemical Process Principles, Part 3: Kinetics and Catalysis, Wiley, New York, 1947, p. 906.
[2] N.A. Katsanos, Ch. Vassilakos, J. Chromatogr. 557 (1991) 469.
[3] Ch. Vassilakos, N.A. Katsanos, A. Niotis, Atmos. Environ. 26A (1992) 219.
[4] J.R. Conder, C.L. Young, Physicochemical Measurement by Gas Chromatography, Wiley, Chichester, 1979.
[5] R.J. Laub, R.L. Pecsok, Physicochemical Applications of Gas Chromatography, Wiley, New York, 1978.
[6] M. Suzuki, J.M. Smith, Adv. Chromatogr. 13 (1975) 213.
[7] N.A. Katsanos, Flow Perturbation Gas Chromatography, Marcel Dekker, New York, 1988.
[8] J.C. Giddings, S.L. Seager, J. Chem. Phys. 33 (1960) 1579.
[9] V.R. Maynard, E. Grushka, Adv. Chromatogr. 12 (1975) 99.
[10] J. Bohemen, J.H. Purnell, J. Chem. Soc. (1961) 360.
[11] P. Fejes, L. Czaran, Hung. Acta Chim. 29 (1961) 171.
[12] J.H. Knox, L. McLaren, Anal. Chem. 36 (1964) 1477.
[13] J.K. Karr, D.T. Sawyer, Anal. Chem. 36 (1964) 1753.
[14] R.P.W. Scott, in: J.H. Purnell (Ed.), Progress in Gas Chromatography, vol. 6, Interscience, 1968, p. 271.
[15] L.S. Ettre, L. Major, J. Takàcs, Adv. Chromatogr. 8 (1969) 271.
[16] N.A. Katsanos, G. Karaiskakis, D. Vattis, A. Lycourghiotis, Chromatoraphia 14 (1981) 695.
[17] N.A. Katsanos, G. Karaiskakis, J. Chromatogr. 254 (1983) 15.
[18] N.A. Katsanos, G. Karaiskakis, J. Chromatogr. 237 (1982) 1.
[19] F. Obberhettinger, L. Badii, Tables of Laplace Transforms, Springer-Verlag, New York, 1973.
[20] R.B. Bird, W.E. Stewart, E.N. Lightfoot, Transport Phenomena, Wiley, Chichester, 1960.
[21] E.N. Fuller, P.D. Schettler, J.C. Giddings, Ind. Eng. Chem. 58 (1966) 19.
[22] T.R. Marrero, R.H. Luecke, AIChE J. 42 (1996) 2365.

[23] J.C. Giddings, Dynamics of Chromatorapy, Marcel Dekker, New York, 1965, p. 239.
[24] G. Karaiskakis, N.A. Katsanos, A. Niotis, Chromatoraphia 17 (1983) 310.
[25] H.J. Arnikar, T.S. Rao, K.H. Karmarkar, J. Chromatogr. 26 (1967) 30.
[26] H.J. Arnikar, T.S. Rao, K.H. Karmarkar, Ind. J. Electronics 22 (1967) 381.
[27] N.A. Katsanos, Ch. Vassilakos, J. Chromatogr. 471 (1989) 123.
[28] F. Dondi, A. Betti, G. Blo, C. Bighi, Anal. Chem. 53 (1981) 496.
[29] F. Dondi, Anal. Chem. 54 (1982) 473.
[30] F. Dondi, F. Pulidori, J. Chromatogr. 284 (1984) 293.
[31] F. Dondi, M. Remelli, J. Phys. Chem. 90 (1986) 1885.
[32] F. Dondi, G. Blo, M. Remelli, P. Reschiglian, in: F. Dondi, G. Guiochon (Eds.), Theoretical Advancement in Chromatography and Related Separation Techniques, Kluwer, Dordrecht, 1992, pp. 173–210.
[33] A. Betti, F. Dondi, G. Blo, S. Coppi, G. Cocco, J. Chromatogr. 259 (1983) 433.
[34] M. Remelli, G. Blo, F. Dondi, M.C. Vidal-Madjar, G. Guiochon, Anal. Chem. 61 (1989) 1489.
[35] N.A. Katsanos, J. Kapolos, Anal. Chem. 61 (1989) 2231.
[36] A. Niotis, N.A. Katsanos, Chromatoraphia 34 (1992) 398.
[37] P.V. Danckwerts, Gas Liquid Reactions, McGraw-Hill, New York, 1970, p. 15.
[38] M. Roth, J. Microcolumn Sep. 3 (1991) 173.
[39] M. Roth, J.L. Steger, M.V. Novotny, J. Phys. Chem. 91 (1987) 1645.
[40] A.V. Kiselev, Ya.I. Yashin, Gas Adsorption Chromatography, Plenum Press, New York, 1969.
[41] N.A. Katsanos, A. Lycourghiotis, A. Tsiatsios, J. Chem. Soc. Faraday Trans. 1(74) (1978) 575.
[42] S.K. Milonjic, M.M. Copecni, Chromatographia 19 (1984) 342.
[43] C. Vidal-Madjar, E. Bekassy-Molnar, J. Phys. Chem. 88 (1984) 232.
[44] J.H. de Boer, The Dynamic Character of Adsorption, Clarendon Press, Oxford, 1953, p. 49.
[45] J. Zeldowitch, Acta Phys. Chim. URSS 1 (1935) 961.
[46] G. Karaiskakis, A. Lycourghiotis, N.A. Katsanos, Z. Phys. Chem. (N.F.) 111 (1978) 207.
[47] C. Vidal-Madjar, G. Guiochon, Bull. Soc. Chim. Fr. (1966) 1096.
[48] A.V. Kouznetsov, G. Guiochon, J. Chim. Phys. 66 (1969) 257.
[49] A.V. Kouznetsov, C. Vidal-Madjar, G. Guiochon, Bull. Soc. Chim. Fr. (1969) 1440.
[50] C. Vidal-Madjar, L. Jacob, G. Guiochon, Bull. Soc. Chim. Fr. (1971) 3105.
[51] C. Vidal-Madjar, G. Guiochon, Bull. Soc. Chim. Fr. (1971) 3110.
[52] G. Blu, L. Jacob, G. Guiochon, J. Chromatogr. 61 (1971) 207.
[53] C. Devillez, C. Eon, G. Guiochon, J. Colloid Interface Sci. 49 (1974) 232.
[54] C. Vidal-Madjar, M.F. Gonnord, G. Guiochon, Adv. Chromatogr. 13 (1975) 177.
[55] C. Vidal-Madjar, M.F. Gonnord, M. Goedert, G. Guiochon, J. Phys. Chem. 79 (1975) 732.
[56] C. Vidal-Madjar, M.F. Gonnord, G. Guiochon, J. Colloid Interface Sci. 52 (1975) 102.
[57] M. Roth, J. Novak, P. David, M. Novotny, Anal. Chem. 59 (1987) 1490.
[58] C.F. Poole, S.K. Poole, Chem. Rev. 89 (1989) 377.
[59] R.N. Nikolov, J. Chromatogr. 241 (1982) 237.
[60] B.R. Kersten, C.F. Poole, J. Chromatogr. 399 (1987) 1.
[61] J.R. Conder, in: F. Dondi, G. Guiochon (Eds.), Theoretical Advancement in Chromatography and Related Separation Techniques, Kluwer, Dordrecht, 1992, pp. 315–337.
[62] J.R. Conder, N.K. Ibrahim, G.J. Rees, G.A. Oweimreen, J. Phys. Chem. 89 (1985) 2571.
[63] J. Janàk, Chromatographia 30 (1990) 489.
[64] C.F. Poole, T.O. Kollie, S.K. Poole, Chromatographia 34 (1992) 281.
[65] G. Park, C.F. Poole, J. Chromatogr. A 726 (1996) 141.
[66] S.K. Poole, T.O. Kollie, C.F. Poole, J. Chromatogr. A 664 (1994) 229.
[67] M.H. Abraham, Chem. Soc. Rev. 22 (1993) 73.
[68] M.H. Abraham, J. Phys. Org. Chem. 6 (1993) 660.
[69] R. Fontaine, C. Pommier, C. Eon, G. Guiochon, J. Chromatogr. 104 (1975) 1.
[70] C. Vidal-Madjar, B.L. Karger, G. Guiochon, J. Phys. Chem. 80 (1976) 394.
[71] V.G. Berezkin, Gas-Liquid-Solid Chromatography, Marcel Dekker, New York, 1991.
[72] L. Sojak, V.G. Berezkin, J. Janàk, J. Chromatogr. 205 (1981) 15.
[73] J. Krupcik, E. Matisova, J. Karaj, L. Sojak, V.G. Berezkin, Chromatographia 16 (1982) 166.
[74] A.R. Dzhumaev, V.G. Berezkin, Zh. Anal. Khim. 46 (1991) 1966.
[75] V.G. Berezkin, A.A. Korolev, Zh. Anal. Khim. 49 (1994) 683.
[76] A. Orav, K. Kuningas, T. Kailas, E. Copliments, S. Rang, J. Chromatogr. A 659 (1994) 143.
[77] V.G. Berezkin, V.P. Pakhomov, V.S. Tatarinskii, V.M. Fateeva, Dokl. Akad. Nauk. SSSR 180 (1968) 1135.
[78] V.G. Berezkin, A.A. Korolev, I.V. Malyukova, J. Microcolumn Sep., in press.
[79] F. Dondi, M.F. Gonnord, G. Guiochon, J. Colloid Interface Sci. 62 (1977) 303.
[80] F. Dondi, M.F. Gonnord, G. Guiochon, J. Colloid Interface Sci. 62 (1977) 316.
[81] R. Madey, P.J. Photinos, D. Rothstein, R. Forsythe, J.-C. Huang, Langmuir 2 (1986) 173.
[82] J.-C. Huang, R. Forsythe, R. Madey, Sep. Sci. Technol. 16 (1981) 475.
[83] V. Sotiropoulou, G.P. Vassilev, N.A. Katsanos, H. Metaxa, F. Roubani-Kalantzopoulou, J. Chem. Soc. Faraday Trans. 91 (1995) 485.
[84] N.A. Katsanos, F. Roubani-Kalantzopoulou, J. Chromatogr. A 710 (1995) 191.

[85] M. Moreau, P. Valentin, C. Vidal-Madjar, B.C. Lin, G. Guiochon, J. Colloid Interface Sci. 141 (1991) 127.
[86] J. Roles, G. Guiochon, J. Chromatogr. 591 (1992) 245.
[87] T. Paryjczak, Gas Chromatography in Adsorption and Catalysis, Ellis Horwood, Chichester, 1986.
[88] M. Jaroniec, R. Madey, Physical Adsorption on Heterogeneous Solids, Elsevier, Amsterdam, 1988.
[89] W. Rudzinski, D.H. Everett, Adsorption of Gases on Heterogeneous Surfaces, Academic Press, New York, 1992.
[90] M. Jaroniec, Adv. Colloid Interface Sci. 18 (1983) 154.
[91] W. Rudzinski, A. Waksmundzki, R. Leboda, Z. Suprynowicz, M. Lason, J. Chromatogr. 92 (1974) 25.
[92] J.P. Hobson, Can. J. Phys. 43 (1965) 1934.
[93] J. Gawdzik, Z. Suprynowicz, M. Jaroniec, J. Chromatogr. 131 (1977) 7.
[94] J. Gawdzik, Z. Suprynowicz, M. Jaroniec, J. Chromatogr. 121 (1976) 185.
[95] Z. Suprynowicz, M. Jaroniec, J. Gawdzik, Chromatographia 9 (1976) 161.
[96] M. Jaroniec, X. Lu, R. Madey, J. Phys. Chem. 94 (1990) 5917.
[97] R.K. Gilpin, M. Jaroniec, M.B. Martin-Hopkins, J. Chromatogr. 513 (1990) 1.
[98] M.B. Martin-Hopkins, R.K. Gilpin, J. Jaroniec, J. Chromatogr. Sci. 29 (1991) 147.
[99] S.P. Boudreau, W.T. Cooper, Anal. Chem. 59 (1987) 353.
[100] J. Jagiello, G. Ligner, E. Papirer, J. Colloid Interface Sci. 137 (1990) 128.
[101] L.B. Harris, Surface Sci. 10 (1968) 128.
[102] J. Roles, G. Guiochon, J. Chromatogr. 591 (1992) 233.
[103] B. Stanley, G. Guiochon, J. Phys. Chem. 97 (1993) 8098.
[104] S. Golshan-Shirazi, G. Guiochon, J. Chromatogr. A 670 (1994) 1.
[105] B.J. Stanley, G. Guiochon, Langmuir 10 (1994) 4278.
[106] B.J. Stanley, G. Guiochon, Langmuir 11 (1995) 1735.
[107] I. Quinoñes, G. Guiochon, J. Colloid Interface Sci. 183 (1996) 57.
[108] M. Heuchel, M. Jaroniec, R.K. Gilpin, J. Chromatogr. 628 (1993) 59.
[109] D.W. Bassett, H.W. Habgood, J. Phys. Chem. 64 (1960) 769.
[110] J. Kallen, E. Heilbronner, Helv. Chim. Acta 43 (1960) 489.
[111] S.H. Langer, J.Y. Yurchak, J.E. Patton, Ind. Eng. Chem. 61 (1969) 10.
[112] E. Gil-Av, Y. Herzberg-Minzly, J. Chromatogr. 13 (1964) 1.
[113] G.L. Pratt, S.H. Langer, J. Phys. Chem. 73 (1969) 2095.
[114] S.H. Langer, J.E. Patton, J. Phys. Chem. 76 (1972) 2159.
[115] S.Z. Roginskii, A.L. Rozental, Dokl. Akad. Nauk. SSSR 146 (1962) 152.
[116] A.D. Berman, M.I. Yanovskii, Dokl. Akad. Nauk. SSSR 197 (1971) 369.
[117] S.Z. Roginskii, A.L. Rozental, Kinet. Catal. 5 (1964) 86.
[118] D. Schweich, J. Villermaux, Ind. Eng. Chem. Fund. 17 (1978) 1.
[119] D. Schweich, J. Villermaux, M. Sardin, AIChE J. 26 (1980) 477.
[120] M. Kocirik, J. Chromatogr. 30 (1967) 459.
[121] M. Suzuki, J.M. Smith, Chem. Eng. Sci. 26 (1971) 221.
[122] M. Suzuki, J.M. Smith, Adv. Chromatogr. 13 (1975) 213.
[123] K. Yamaoka, T. Nakagawa, J. Chromatogr. 105 (1975) 225.
[124] R. Thede, H. Pscheidl, D. Haberland, Z. Phys. Chem. (Leipzig) 266 (1985) 1089.
[125] R.A. Keller, J.C. Giddings, J. Chromatogr. 3 (1960) 205.
[126] M. Jung, V. Schurig, J. Am. Chem. Soc. 114 (1992) 529.
[127] W. Bürkle, H. Karfunkel, V. Schurig, J. Chromatogr. 288 (1984) 1.
[128] D.H. Hochmuth, W.A. König, Liebigs Ann. Chem. (1996) 947.
[129] J. Veciana, M.I. Crespo, Angew. Chem. 103 (1991) 85.
[130] D. Schweich, J. Villermaux, Ind. Eng. Chem. Fund. 21 (1982) 47; ibid. 21 (1982) 51.
[131] P.W. Carr, in: G. Ganetsos, P.E. Barker (Eds.), Preparative and Production Scale Chromatography, Marcel Dekker, New York, 1993, p. 421.
[132] L.G. Harrison, Y. Koga, J. Chromatogr. 52 (1970) 39.
[133] P. Schulz, Anal. Chem. 47 (1975) 1979.
[134] R. Thede, E. Below, H. Pscheidl, D.J. Haberland, J. Chromatogr. 520 (1990) 109.
[135] R. Thede, D. Haberland, Z. Deng, S.H. Langer, J. Chromatogr. A 683 (1994) 279.
[136] S.H. Langer, J.E. Patton, in: J.H. Purnell (Ed.), New Developments in Gas Chromatography, Wiley, New York, 1973, pp. 294–373.
[137] C.-Y. Jeng, S.H. Langer, J. Chromatogr. 589 (1992) 1.
[138] R. Thede, H. Pscheidl, D. Haberland, Z. Phys. Chem. (Leipzig) 271 (1990) 471.
[139] M. Czok, G. Guiochon, Anal. Chem. 62 (1990) 189.
[140] L. Bachmann, E. Bechthold, E. Cremer, J. Catal. 1 (1962) 113.
[141] G.A. Gaziev, V.Y. Filinovski, M.I. Yanovski, Kinet. Catal. 4 (1963) 599.
[142] V.G. Berezkin, V.S. Kruglikova, N.A. Belikova, Dokl. Akad. Nauk. SSSR 158 (1964) 182.
[143] V.Y. Filinovski, G.A. Gaziev, M.I. Yanovskii, Dokl. Akad. Nauk. SSSR 167 (1966) 143.
[144] V.G. Berezkin, V.S. Kruglikova, V.E. Shiryayeva, Teor. Eksp. Khem. 3 (1967) 553.
[145] S.H. Langer, J.Y. Yurchak, C.M. Shaughnessy, Anal. Chem. 40 (1968) 1747.
[146] L.G. Harrison, Y. Koga, P. Maddderom, J. Chromatogr. 52 (1970) 31.
[147] M.I. Yanovskii, A.D. Berman, J. Chromatogr. 69 (1972) 3.
[148] J.E. Patton, H. Kung, S.H. Langer, J. Chromatogr. 104 (1975) 73.
[149] A.E. Mysak, Y.A. Kanchenko, V.G. Berezkin, N.P. Mysak, Kinet. Catal. 16 (1975) 257.
[150] A.N. Genkin, N.A. Petrova, J. Chromatogr. 105 (1975) 25.
[151] B.D. Unger, R.G. Rinker, Ind. Eng. Chem. Fund. 15 (1976) 225.
[152] S.H. Langer, H.R. Melton, T.D. Griffith, J. Coca, J. Chromatogr. 122 (1976) 487.
[153] M. Pank, A. Kogerman, O. Kirret, G. Rajalo, J. Chromatogr. 119 (1976) 409.
[154] T.D. Griffith, A.H.T. Chu, S.H. Langer, Chem. Eng. J. 36 (1987) 73.

[155] P. Antonucci, N. Giordano, J.C. Bart, J. Chromatogr. 150 (1978) 309.
[156] B. Mile, L. Morton, P.A. Sewell, J. Chromatogr. 204 (1981) 5.
[157] H. Pscheidl, E. Möller, D. Haberland, Mitteil. Chem. Ges. 28 (1981) 31.
[158] T. Petroulas, R. Aris, R.W. Carr, Chem. Eng. Sci. 40 (1985) 2233.
[159] J.B. Powell, C.Y. Jeng, S.H. Langer, Chem. Eng. Sci. 42 (1987) 1797.
[160] A.F. Shushunova, J. Chromatogr. 365 (1986) 417.
[161] J. Coca, G. Adrio, S.H. Langer, Chem. Eng. Sci. 43 (1988) 2007.
[162] R. Thede, F. Nohmie, H. Pscheidl, D. Haberland, Z. Phys. Chem. 173 (1991) 87.
[163] B.B. Fish, R.W. Carr, Chem. Eng. Sci. 44 (1989) 1773.
[164] J.A. Dinwiddie, W.A. Morgan, US Patent, 2 976132, 1961.
[165] E. Gil-Av, Y. Herzberg-Minzly, Proc. Chem. Soc. (1961) 316.
[166] V. Schurig, M. Jung, M. Schleimer, F.-G. Klärner, Chem. Ber. 125 (1992) 1301.
[167] R. Thede, E. Below, D. Haberland, J.A. Jönsson, J. Liq. Chromatogr. 18 (1995) 1137.
[168] J. Coca, M. Bravo, E. Abscal, G. Adrio, Chromatographia 28 (1989) 300.
[169] O. Pazdernik, P. Schneider, J. Chromatogr. 207 (1981) 181.
[170] B. Stephan, H. Zimmer, F. Kastner, A. Mannschreck, Chimia 44 (1990) 336.
[171] C.S.G. Phillips, A.J. Hart-Davis, R.G.L. Saul, J. Wormald, J. Gas Chromatogr. 5 (1967) 424.
[172] N.A. Katsanos, A. Lycourghiotis, Chim. Chronika (New Series) 5 (1976) 137.
[173] N.A. Katsanos, J. Chromatogr. 152 (1978) 301.
[174] I. Hadzistelios, H.J. Sideri-Katsanou, N.A. Katsanos, J. Catal. 27 (1972) 16.
[175] A. Lycourghiotis, N.A. Katsanos, I. Hadzistelios, J. Catal. 36 (1975) 385.
[176] A. Lycourghiotis, N.A. Katsanos, Reaction Kinet. Catal. Lett. 4 (1976) 221.
[177] A. Lycourghiotis, N.A. Katsanos, D. Vattis, J. Chem. Soc. Faraday Trans. 1(75) (1979) 2481.
[178] A. Lycourghiotis, D. Vattis, N.A. Katsanos, Z. Phys. Chem. (N.F.) 126 (1981) 259.
[179] A. Tseremegli, N.A. Katsanos, I. Hadzistelios, Z. Phys. Chem. (N.F.) 129 (1982) 21.
[180] N.A. Katsanos, A. Tsiatsios, J. Chromatogr. 213 (1981) 15.
[181] D. Vattis, N.A. Katsanos, G. Karaiskakis, A. Lycourghiotis, M. Kotinopoulos, J. Chromatogr. 214 (1981) 171.
[182] J.P. Powell, S.H. Langer, J. Catal. 94 (1985) 566.
[183] I. Topalova, A. Niotis, N.A. Katsanos, V. Sotiropoulou, Chromatographia 41 (1995) 227.
[184] A.J. Sedman, J.G. Wagner, J. Pharm. Sci. 65 (1976) 1006.
[185] Ch. Abatzoglou, E. Iliopoulou, N.A. Katsanos, F. Roubani-Kalantzopoulou, A. Kalantzopoulos, J. Chromatogr. A 775 (1997) 211.
[186] H. Zahariou-Rakanta, A. Kalantzopoulos, F. Roubani-Kalantzopoulou, J. Chromatogr. A 776 (1997) 275.